Chapter 9
On-site Monitoring of Mass Concrete

Dirk Schlicke, Fragkoulis Kanavaris, Rodrigo Lameiras and Miguel Azenha

Abstract On-site monitoring of mass concrete offers several benefits. It may comprise a wide range of objectives from (i) the maintaining of adequate temperature conditions for the evolution of the desired concrete properties and to (ii) the determination of thermal and mechanical parameters for verification of the calculation models and assumptions applied for crack assessment of the considered structure. Next to very general information on monitoring of mass concrete, this chapter presents different levels of measures with regard to the purpose and expected insights into each level, available instruments and least requirements on practical application, as well as possibilities for result verification. The chapter focuses on both established techniques with comprehensive experiences in many applications and comparably new techniques available on the market. Finally, the presented techniques and approaches were exemplified on three different application examples with regard to different measurement systems as well as types of structures.

D. Schlicke (✉)
Graz University of Technology, Graz, Austria
e-mail: dirk.schlicke@tugraz.at

F. Kanavaris
Queen's University of Belfast, Belfast, UK

R. Lameiras
University of Brasília (UnB), Brasília, Brazil

M. Azenha
ISISE, University of Minho, Guimarães, Portugal

E. M. R. Fairbairn and M. Azenha (eds.), *Thermal Cracking of Massive Concrete Structures*, RILEM State-of-the-Art Reports 27,
https://doi.org/10.1007/978-3-319-76617-1_9

9.1 General Basics

9.1.1 Opportunities and Limitations of On-site Monitoring of Mass Concrete

An important outcome of mass concrete monitoring is the confirmation that adequate conditions for the evolution of the desired concrete properties were maintained. This refers to both the assurance of a correct hydration process within the limits of acceptable maximum concrete temperature as well as the avoidance of harmful temperature-induced cracking. The latter results from high temperature gradients between interior and surface of a lift as well as high temperature differences between the lift and neighbouring construction stages. Next to temperature measurements, monitoring of mechanical parameters provides also insights into strains or even stresses in the concrete. This enables, in combination with temperature measurements, a reliable database for further considerations. Besides, the measurement results provide important data to verify the calculation models and assumptions applied for crack assessment of the considered structure, as well as to improve these calculation models and assumptions for future projects.

Providing an appropriate measurement as well as correct analysis, it can be said that precision and reliability of the drawn conclusions correlate with the extent of monitoring measures applied. This means, e.g., solely measuring the temperature in a single point of the cross section requires further assumptions to draw conclusions on the temperature field of the member and solely measuring temperature—even with adequate number of measuring points in the cross section—requires further assumptions to quantify strains or even stresses and crack risk of the structure.

In general, the extent of monitoring measures should always be determined according to the intended insight. Of course, cutbacks are possible and often reasonable as well. Realistic assumptions and experience can also ensure meaningful and correct conclusions; however, it should always be kept in mind that such conclusions rely on the quality of the assumptions and might therefore be defective.

At this point, it should also be mentioned that measurement results and conclusions drawn are always subject to uncertainties. The main reasons are: (i) measurement uncertainties of the applied method, (ii) the influence of the presence of a sensor in the measurement environment and (iii) the need of additional assumptions to relate the measurement value correctly to the real concrete behaviour. These aspects will be addressed accordingly in the following presentation of available monitoring techniques.

9.1.2 Set-up of an On-site Monitoring

On-site monitoring of mass concrete aims to obtain maximum values of a given parameter, e.g. temperature, strain, but also to determine the distribution of such parameter within the monitored member and its evolution throughout time. Common sampling rates according to recently reported monitoring programmes are at least one sampling per hour or more (e.g. RILEM 1998; Morabito 2001; Azenha 2009; Schlicke 2014; Soutsos et al. 2016; Kanavaris 2017). Besides, it is of crucial importance to adequately record the relevant environmental conditions, which will be discussed in Sect. 9.2.

The positioning of sensors within the member should enable the prior mentioned aims: knowing peak values and their distribution in space. This can be achieved by sensor arrangement along the main axes of changes, e.g. over height and width of the member. According to Schlicke (2014), the number of required sensors along those axes should be determined with respect to the shape of the parameter distribution to be observed. Parabolic shapes, for instance, would require a minimum of three sensors over the width, whereas shapes of higher order require more sensors.

Besides, the positioning of sensors needs to respect least requirements of each sensor type in terms of minimum concrete cover as well as minimum distances between sensors. In general, this refers to a possible affecting of the concrete behaviour due to the presence of too many sensors in a too small area, mainly in regard to the disturbance of the strain field due to the presence of concrete embedment strain gauges or stressmeters with even higher influence on the surrounding. If in doubt, preliminary studies of the disturbed strain field can provide further information to find an optimal solution. Although specific reports of such procedure could not be found in the literature, a possible approach applied in the preparation of several on-site monitoring in the context of Schlicke (2014) should be outlined here. In these studies, the effect on the strain field was determined with FE studies by putting a representative void in a volume and shortening the volume. The conclusion was drawn from the change of the strain field since the sensor works are also strain-based. For low stiffness concrete embedment strain gauges with an inner diameter of the connection pipe of <2 mm, such FE studies showed that the influence of the presence of the sensor on the strain field of the cross section is smaller than 1% as long as the cover is >5 cm or the minimum distance between concrete embedment strain gauges is >10 cm.

For illustrative purposes, Fig. 9.1 summarizes the above-discussed points regarding the positioning of sensors in a general manner.

The illustration in Fig. 9.1 shows a proposal for sensor positioning in a more block-shaped member without a clear length direction. In these types of members, the parameters to be monitored show usually a volumetric distribution so that sensor arrangement is required in all three dimensions. One simplification could be the usage of symmetry over the depth if front and backside show comparable conditions. On the contrary, if the member to be monitored can be categorized as

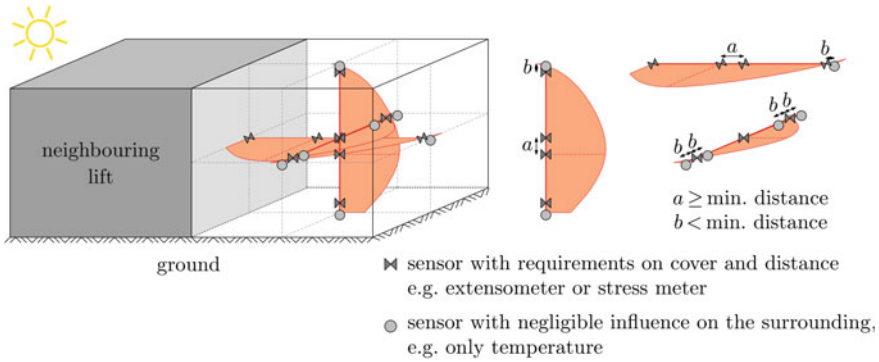

Fig. 9.1 Requirements on sensor positioning

slab or as wall, the number of sensors can be reduced further. As outlined in Schlicke (2014), slabs can be adequately monitored by a measurement chain over the height in a single point, whereas walls can be adequately monitored by a sensor arrangement in the decisive cross section in length direction. The reason is that parameters to be monitored are almost constant over the member length and in case of slabs also over the width, as exemplified in Fig. 9.2.

Other important aspects are cable routing and data logging. Common temperature monitoring can be seen as state of the art. There are numerous loggers designed to record temperature data, providing a variety in logger capabilities, such as power or battery operation, battery life, stand-alone or computer controlled thermocouple compatibility. Some examples were shown in Fig. 9.3.

With increasing extent of the monitoring programme, extensive cable routing and demanding data logging can become a challenging task and need to be handled with care. In case of electronic sensors, an increasing number of sensors cause significant cable bundles which could affect the measurement environment. Besides, professional data loggers with multiplexing properties are needed. Figure 9.4 shows the cable bundles of the monitoring programme of a 4.0-m-thick power plant slab as well as the installation of the data logger on the top surface of

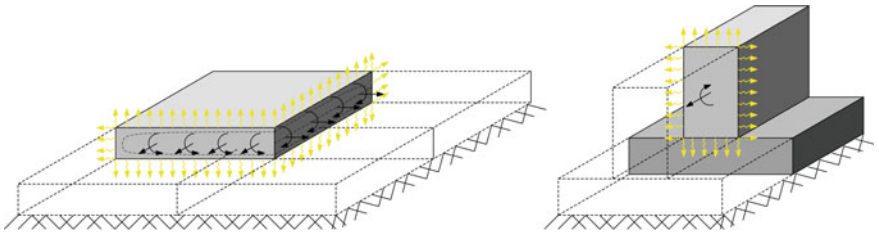

Fig. 9.2 Member types with areal distribution of parameters to be monitored (Schlicke 2014)

(a) dataTaker DT85M
(photo: M. Azenha)

(b) Pico TC-8
(photo: F. Kanavaris)

(c) Ahlborn ALMEMO 3290 V5
(photo: D. Schlicke)

(d) Gant Squirrel OQ610-S
(photo: F. Kanavaris)

Fig. 9.3 Example of temperature data loggers

Fig. 9.4 Cable routing and arrangement of the data logger in the monitoring programme of the 4.0-m-thick power plant slab Boxberg (*Photos* D. Schlicke)

the slab. To protect the cable bundles from damage during casting, the cables were routed along the reinforcement mesh and finally guided in the inside of a steel pipe. Another important aspect is the sensitivity of electrical measurements against electrical disturbances due to welding on-site. Thus, especially construction sites with excessive arc welding activities require an independent grounding of the measurement installation.

Fibre optical measurements have advantages in regard to both insensitivity against electrical disturbances due to welding on-site as well as cable routing since

sensors can be connected serially. In the best case only one wire is needed (e.g. Humar et al. 2016; Bao and Chen 2012), but it should be noted that serially connected sensors cannot be controlled absolutely simultaneously. Depending on the scanning speed of the chosen system, a certain delay of measuring times between the sensors has to be accepted (Delsys 2017; Emilio 2013). Besides, an application with several independent wires which are controlled by only one interrogator causes time shifts between the exact measuring times of the sensors. The reason is the required time for signal processing before switching to the next cable; however, if measurement results are required at exactly the same, time this circumstance may be overcome by fitting of the result curves.

Recent advancements in concrete temperature monitoring also include wireless systems. Several efforts have been made to develop wireless systems based on various operating principles to enable the wireless evaluation of temperature history of concrete; see Kim et al. (2015), Lee et al. (2014), Barroca et al. (2013), Chang and Hung (2012), Noris et al. (2008). In addition to that, such systems have been recently commercialized and offer remote evaluation of the temperature and strength development in concrete structures, with their potential limitations described in Soutsos et al. (2016, 2017), Kanavaris (2017), Vollpracht et al. (2018).

It is also important to take into account the need to host the data logger in the vicinity of the actual construction. Mass concrete structures are frequently built-in remote areas or areas where there are no adjacent buildings, at least. Special care needs to be taken in regard to four main situations: (i) risk of theft or vandalism; (ii) need to shield the data logger from environmental action; (iii) ensuring a stable source of electricity; and (iv) usual need for a stand-alone solution that does not depend on a computer, which is bulky and an additional attractor for potential theft situations. The solution found by the team at the University of Minho (Costa 2011; Azenha et al. 2014) counteracts the four above-mentioned threats with a set of combined actions:

(i) In order to counteract theft/vandalism issues, or even damages due to curiosity of people passing by, the data logger and all connection hubs are hosted inside a robust electrician box. The box is screwed through the inside to a wall and closed with a key and external locker. This makes it very hard for anyone without the key to open the box or even remove it from the wall into which it is fixed. Care must also be taken to ensuring some fixing devices in between the data logger and the cables accessible from the outside: if someone pulls the cables from the outside (either on purpose or by chance), the corresponding force should not be exerted directly on the wiring connections of the data logger. On the contrary, it ends up being absorbed by the fixing device inside the box. No vandalism acts were recorded even in areas that are easily accessible by general public. However, there are cases in which wires can be incidentally cut.

(ii) In order to shield the data logger from outer environmental action, such as rain/snow, the electrician box (or similar) should be water tight, as shown in the door/opening of Fig. 9.5, which interpenetrate with a sealant rubber. In

(a) Data logger and battery inside the box *(b) Impermeable electric box with data logger inside*

Fig. 9.5 Data logger positioning and sheltering (Costa 2011; Azenha et al. 2014)

the event of heavy rain, there were no leakage events observed. Furthermore, the holes for the cabling are always made from the bottom surface of the bounding box, as to make sure that no entry of rain/snow happens. The hole should also be as tight as possible to the cables, as to avoid mice or other small animals or insects from coming in. In spite of such care, regular inspections should be done to the state of cables, data logger and bounding box.

(iii) Experience of the team at the University of Minho (Costa 2011; Azenha et al. 2014) has shown that power outages and surges are frequent in construction sites. Therefore, the system should be made independent of such type of problems that may cause disturbances on measurements, or even interruptions of measurement and ultimately damages to the data logger. To circumvent such problem, batteries are normally used to power the data logger; see the black box in Fig. 9.5. Even though this brings great advantages to the stability of electricity signals, it carries the downside of requiring regular replacement of the battery by a newly charged one. In the context of monitoring of mass concrete in few weeks processes, this is normally not a problem, as the consumption of the data logger tends to be small, and battery may withstand for several weeks without needing to be recharged.

(iv) Data loggers with stand-alone operation mode at low electricity consumption and large capacity to store data (USB flash drives) are normally desirable in this type of application. There are several options in the market that satisfy

these criteria. This extends the life of the battery, eliminates the need to extract data to avoid "full memory problems" and removes the need for a highly consuming computer, which is simultaneously the type of item that is rather prone to induce thefts.

Another important matter pertains to the support of sensors in the context of mass concrete structures. Indeed, there are many regions of mass concrete that are totally unreinforced (core, for example). In such cases, when measurements are intended, the support of sensors at predefined locations becomes an issue. As reported by Azenha (2009), this may be overcome by placing specific supports for this matter. Such do not have any special requirements, except for: (i) they must not induce fragilities or compatibility/durability issues in the mass concrete element; (ii) they must be stiff enough to ensure adequate location and direction of the sensors themselves throughout the operations of casting; and (iii) they must not significantly affect the temperature field. An example of such type of system can be seen in Fig. 9.6, where measurement of temperature and strain is illustrated with vibrating wire strain gauges in a core region of mass concrete. In such example, a staged construction dam is shown, with casting heights of 1.2 m. The PVC pipes were embedded by 1.2 m in the previous casting stage (present during the casting itself) and extended further 1.2 m in correspondence with the subsequent casting stage. Before the subsequent casting stage, the pipes were connected to each other by steel bars that simultaneously braced the pipes to each other and allowed the support of the sensors themselves at the desired heights of monitoring. Besides, the pipes were prefilled with mortar in order to reduce thermal influences due to the voids.

After completion of the monitoring, the embedded sensors remain in the concrete, whereas all external parts of the installation were usually dismantled. However, it might be recommended that the monitoring set-up provides also proper preservation of the cable ends during service life, rather than just being cut-off from

(a) vertical supports *(b) horizontal supports*

Fig. 9.6 Supports tailored for allowing vertical profiling of temperatures and strain in unreinforced regions of mass concrete (Azenha 2009; Azenha et al. 2014)

hardened concrete and sealed. This enables future assessments of the structure at later ages, even if long-term monitoring is not being considered at the moment.

9.1.3 Calibration of Sensors

Adequate calibration of the sensors is important and should be handled with care to ensure technically reliable measurements. Usually, sensors were calibrated against reference values, e.g. calibrating temperature sensors using 0 °C as reference point by inserting the sensor into an ice bath, as depicted in Meanset (2009). Further information can be found in ASTM (1993, 2015), EURAMET (2011) as well as in the individual specifications of the applied sensors.

9.1.4 Analysis of Results

Basically, the measurement results represent the state or course in time of the determined parameter (temperature, humidity, strain, stress, etc.) in single points of the cross section. With respect to the whole cross section, each parameter is distributed with a certain shape (e.g. temperature field or strain field). As outlined in Schlicke (2014) and shown in Schlicke (2015), detailed conclusions on structural behaviour require both to derive the field from the punctual measurement results and to identify characteristic parts in the field for further conclusions. In accordance with the common understanding, these characteristic parts are: (i) constantly in the whole cross-sectional distributed part; (ii) linearly over width and height of the cross-sectional distributed parts as well as (iii) the residual part, which is usually nonlinearly distributed and self-balanced within the cross section. Figure 9.7 illustrates this context; further information is given in, e.g., Schlicke and Tue (2015), Heinrich and Schlicke (2016), Eierle and Schikora (2000), Rostásy and Hennig (1990) or Reinhardt (2014).

Besides spatial aspects, the interpretation and further processing of measurement results can require time discrete and incremental analysis as well. One example is

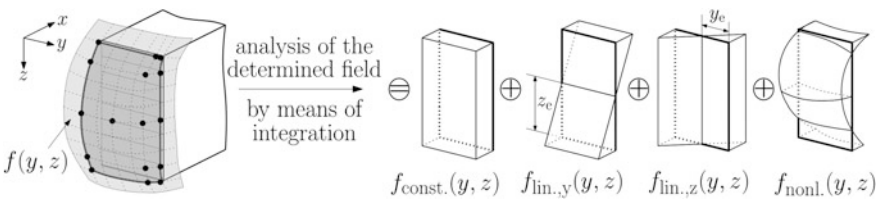

Fig. 9.7 Determination of the cross-sectional distribution $f(y, z)$ of the measurand out of punctual measurement results (•) and analysis of the determined field

the conclusion from measured strains to stresses, whereby several simultaneously evolving concrete properties in the course of time as well as the superposition with viscoelastic effects occurring by time need to be considered. As shown in Schlicke (2014), this can be achieved by splitting the course of time into time steps and adding up the changes of each time step to a course over time. Figure 8.12 in Chap. 8 gives an impression of such procedure.

The beginning of the monitoring is usually determined by the placement of concrete. In terms of temperature monitoring, this is usually witnessed by the person responsible for the monitoring. However, strain measurements require a clear definition of the beginning of reliable results with respect to the setting time, as reported in Azenha et al. (2014).

9.1.5 Verification

In the literature, different ways for the verification of monitoring results can be found. This refers mainly to:

1. Comparison of monitoring results with independently obtained measurements,
2. Comparison of monitoring results with results of computational simulations and
3. Compatibility check of monitoring results among each other.

The first point, comparison of monitoring results with independently obtained measurements, refers either to all cases in which third-party data is applied for verification, e.g. comparison of recorded environmental conditions on-site with data of nearby weather stations, or to all cases in which redundant measurement results within the monitoring were compared to each other. The latter is typical for verification of novel monitoring techniques, such as sensing of temperature in the concrete along optical fibres verified with conventional measurements of concrete temperature with sensors at single points.

The second point, comparison of monitoring results with results of computational simulations, refers to all kinds of monitoring results ranging from temperature development, overstrain histories up to stress development in the concrete. Such procedure is often applied, e.g. Azenha et al. (2009, 2017), Lawrence et al. (2012), Rostásy et al. (2007), Schlicke (2014, 2015), Kanavaris (2017). For illustrative purposes, Fig. 9.8 shows the results of the computational simulation of monitored temperature, strains and stresses of the prior mentioned power plant slab Boxberg.

Computational simulations, however, are always subject to the reliability of the material model and the calculation assumptions. Of course, the computational simulation of concrete temperature by means of analytical equations, e.g. Bamforth (2007), Riding et al. (2006), or by application of time discrete thermodynamic models, as presented in Chap. 7 of this report, provides usually reliable proof. The computational simulation of monitored strains and stresses, however, underlies a complex interplay between the thermomechanical material behaviour including

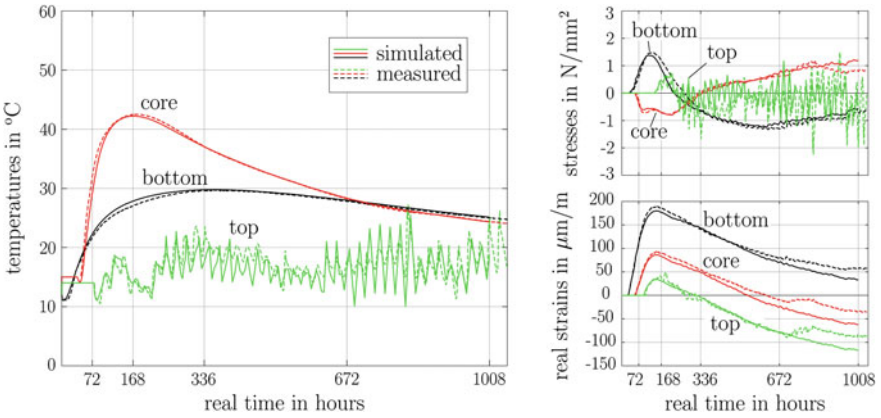

Fig. 9.8 Example of computational simulation of measurement results in the 4.0–m-thick power plant slab Boxberg (Schlicke 2014)

viscoelastic effects as well as the calculation assumptions. According to Schlicke (2014), unequivocal verification is therefore only provided if calculation results agree satisfactorily with the determined real deformation and stress history at the same time, as shown in Fig. 9.8.

The third point, compatibility check of monitoring results among each other, refers to check whether monitored temperature, strains as well as stresses are compatible with each other in the course of time. A mandatory requirement of this procedure is therefore the monitoring of all three parameters in comparable points of the structure, and it is usually limited to the uncracked state. Basically, such procedure was already proposed by Raphael and Carlson (1965) with the "combination of stressmeters and strain metres for completely independent check". A recent report of such procedure can be found in Schlicke (2014), whereby the verification was considered as successful if the monitored stress history could be retraced quantitatively over the course of time by the monitored strain history. For the purpose of illustration, Fig. 9.9 depicts the result of the compatibility check of the above-mentioned monitoring of the ground slab Boxberg.

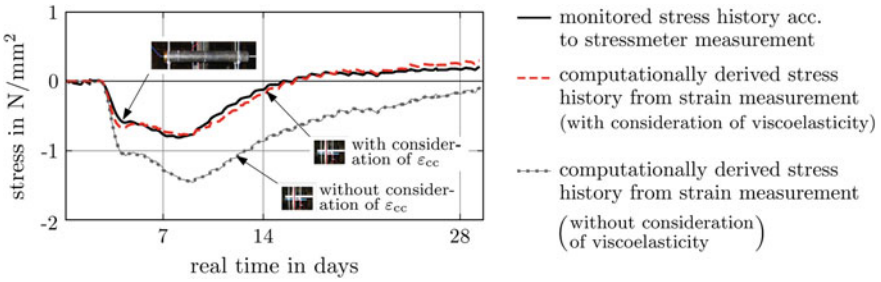

Fig. 9.9 Determined stresses on half height of the slab: comparison between stressmeter results and computational derivation from strain measurement (Schlicke 2014)

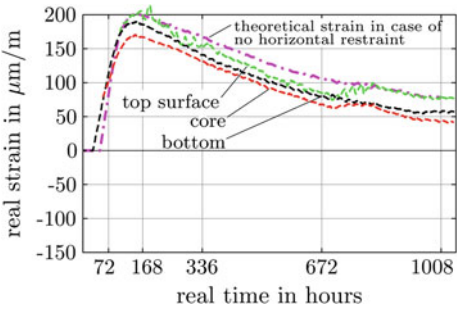

Fig. 9.10 Determined strains over the height of the slab (shifted at setting time to the present strain of the slab) and comparison with constant part of temperature field (Schlicke 2014)

Besides, the analysis of the obtained real strains enables a broader checking of the coherence of the monitoring. For instance, the theoretical axial elongation or shortening of the member according to thermal expansion and shrinkage can be compared with the real strain in each measuring point, whereby the difference between them should be in line with the expected restraint degree in axial direction (Austin et al. 2006; Schlicke 2014, 2015). Besides, the analysis of real strain measurements over the member height provides insights into the extent of self-weight activation due to temperature and/or moist gradients over the member height and whether the cross section remains even or not (Schlicke 2014, 2015). Figure 9.10 depicts such comparison for the above-mentioned monitoring of the ground slab Boxberg. In this example, the layerwise casting of the slab required the consideration of accordingly delayed setting of each casting layer. The strain history of each measuring point was therefore shifted on the y-axis until its initial value at setting complies with the present strain of the layer below. Altogether, the comparison with the theoretical strain of the whole member in case of no external restraint shows that the slab can deform in axial direction almost freely. On the contrary, the strains over the height are running almost parallel, which indicates a plane cross section as well as full restraint of any curvature.

9.2 Recording of External Conditions

9.2.1 Preliminary Remarks

Monitoring of the environmental conditions on-site refers predominantly to recording of ambient temperature, solar radiation, relative humidity and wind velocity. When it comes to mass concrete pouring and curing, this can provide improvements for three main reasons: (i) obtain the anticipated external conditions prior to concrete pouring in order to avoid critical pouring times regarding risk of cracking occurrence; (ii) monitor the external conditions during concrete pouring and curing to enable taking control measures in situ to mitigate cracking;

and (iii) incorporate the obtained ambient conditions in finite element modelling as input parameters in order to numerically estimate the thermal- and shrinkage-induced stresses in the concrete (e.g. Azenha 2009; Schlicke 2014).

A peculiarity of monitoring on-site is the determination of correct environmental conditions to which the member is exposed to reality. In contrast to meteorological observations, which comply with observation standards, e.g. WMO (2008), the decisive conditions of a member are significantly affected by microclimatic influences as outlined in Nilsson (1996).

Omitting explicit monitoring of on-site conditions and relying solely on meteorological weather data, which is e.g. provided comprehensively in several online weather databases, has to be seen with respect to its limitations. On the one hand, the available meteorological weather data is usually much less detailed over time and solely provided in form of average and min./max. values per day, and on the other hand, the aforementioned microclimatic effects can lead to significant differences between real on-site conditions and external conditions recorded with the nearby weather station. On the contrary, an objective comparison of measurements with meteorological weather data can provide an appropriate opportunity for the verification of the monitoring.

9.2.2 Ambient Temperature

The ambient temperature is usually measured using simple but robust sensors such as thermocouples as these are inexpensive options providing suitable accuracy for the purpose of the monitoring.

With respect to microclimatic effects, special attention is to be given to the location and shielding of the sensor. Regarding the location, two general possibilities exist: (i) the sensor is located very close to the concrete surface recording the temperature of the air which is in direct contact with the concrete, or (ii) the sensor is located away from the concrete surface where the ambient temperature is not affected by surface effects from the concrete, for example, following the placement guidelines outlined in WMO (2008). Both cases are illustrated in Fig. 9.11.

The first possibility provides results which can be used directly as boundary condition for computational simulations but cannot directly be compared with the air temperature as defined by meteorological standards. The second possibility provides an air temperature which could be compared to the air temperature according to meteorological standards, but requires corrections in order for it to be applied as a boundary condition in computational simulations. Both cases, however, need adequate protection of the sensor against radiation and moisture to avoid that solar radiation and/or evaporation on the sensor itself may influence the measurement. Solar radiation will result in an increase of the recorded temperature, whereas moisture (or the presence of fog) can reduce the recorded temperature.

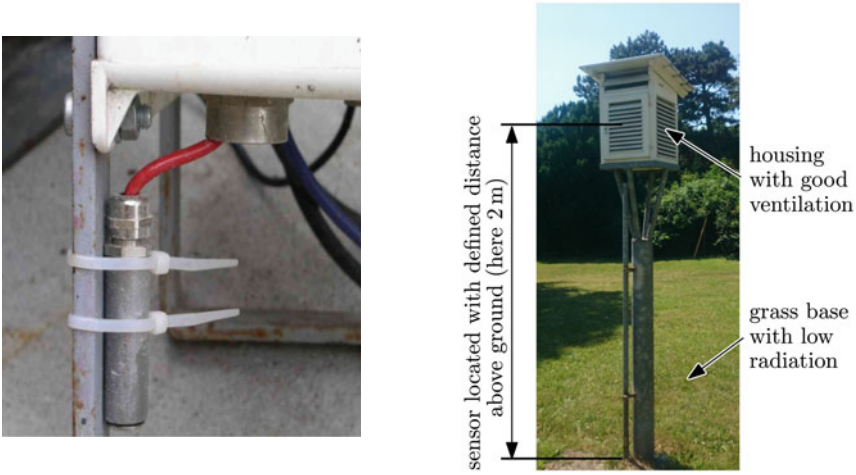

(i) placement close to the concrete surface with shielded sensor

(ii) placement according to meteorological standards, e.g. (WMO 2008)

Fig. 9.11 Measurement of ambient air temperature (*Photographs* D. Schlicke)

9.2.3 Solar Radiation

Solar radiation affects the temperature field of mass concrete in different ways. As outlined in Honorio (2015), Riding et al. (2009), van Breugel (1998), or Bernander (1998), the solar radiation on the final surface induces higher thermal gradients. Next to this, additional heat can also be included during the pouring when concrete is placed in large layers which remain open for a couple of hours (Schlicke 2014). Besides, the knowledge of occurring solar radiation improves the accuracy of calculation models in terms of considered heat transfer by irradiation (Bofang 2014; Riding et al. 2006).

The solar radiation in a horizontal surface is often measured on-site using high-precision sensors known as pyranometers (TGES 2008). There are different types of pyranometers, designed for different purposes, however, for the purpose of measuring the solar radiation on the surface of concrete; a low-cost silicon pyranometer as shown in Fig. 9.12a is usually accurate enough (Azenha 2009). Alternatively, solar radiation can be also measured with the so-called photovoltaic pyranometers, also known as reference cells, which implement a solar (photovoltaic) cell to convert energy of light directly into electricity (Meydbray et al. 2012). An example of a self-built device on basis of a solar cell is shown in Fig. 9.12b. Another opportunity is the application of thermopile pyranometers according to the standard of metrological monitoring, whilst all types of pyranometers are classified into categories in the relevant ISO standard (ISO 1990) in terms of their performance (Paulescu et al. 2013).

(a) commercial silicon pyranometer (Delta Ohm 2017)

(b) self-built device on basis of a solar cell (photo: D. Schlicke)

Fig. 9.12 Measurement instruments for the monitoring of solar radiation

9.2.4 Wind Speed

Wind speed usually fluctuates significantly with time and location, increases with distance from the ground and is affected by the surrounding environment (Burton et al. 2011). Complex fluctuations in wind speed on a fast timescale can also occur as a result of a phenomenon known as turbulence, whilst the effects of turbulence become more pronounced as the height above ground decreases (Burton et al. 2011).

With respect to mass concrete, wind could have a detrimental effect on its performance, as evaporation and cooling of exposed surfaces will rapidly increase due to increased convective and evaporative heat loss (Wojcik et al. 2003; Wojcik 2001), potentially leading to surface cracks from thermal shock or drying, depending on ambient temperature and relative humidity (van Breugel 1998).

In general, wind speed can be measured with anemometers. Among several types of anemometers, see Langreder (2010), Johnston (2005), a simple, robust and appropriate wind speed monitoring can be provided with so-called three- or four-cup anemometers. Relevant details regarding their use, installation and interpretation of results have been reported by Hunter (2003). However, as mentioned earlier there are very complex microclimatic interactions making the precise monitoring of wind at different locations difficult. A reasonable approach for determination of convection coefficients is to refer to simplified mean values or

wind strength scales. The most frequently adopted approach to quantify the wind intensity is the Beaufort wind force scale which is an empirical measure relating wind speed to observed land and sea conditions (Met Office 2010; Mather 2005).

9.2.5 Relative Humidity

It is common understanding that relative humidity is an important parameter of the curing process since moisture loss of the concrete surface is significantly influenced by the value of relative humidity (ACI 2007). However, the on-site monitoring of relative humidity is usually not essential for mass concrete applications. The drying depends predominantly on average conditions of relative humidity (Neville 2011), which can be gathered adequately from nearby weather stations. Nevertheless, if such measurements would be required for special purposes, hygrometers could be applied closely to the concrete surface whilst more detailed information is given elsewhere (Barnes 2016; Simpson 2016; Kanare 2005).

9.2.6 Integrated Monitoring with Weather Stations

In the cases in which a comprehensive gathering of meteorological on-site characteristics is required, weather stations may be also considered. These devices normally comprise of a thermometer for measuring air temperature, a hygrometer for measuring humidity, an anemometer for measuring wind speed, a pyranometer for measuring solar radiation and a rain gauge for measuring liquid precipitation (Davis 2016; WMO 2008). A weather station can be considered as an affordable option which provides a set of useful information, with respect to environmental conditions on-site, and it is particularly convenient as it combines different sensors and instruments in one device.

9.3 Temperature Measurements in the Concrete

9.3.1 Preliminary Remarks

Temperature monitoring within mass concrete provides fundamental information related to concrete performance. Besides the aforementioned detection of temperature maxima as well as temperature gradients, temperature monitoring is nowadays also applied to indirectly conclude on the evolution of strength in order to optimize stripping times or thermal insulation (e.g. Carino and Lew 2001).

There are several temperature sensors available on the market which are suitable for measuring the temperature of hardening concrete, having different operation principles and accuracy. The most commonly used are thermocouples, resistance temperature detectors and thermistors. In case of a longitudinal shape of the sensors or their housing, it is recommended to place near-surface sensors parallel to the exposed surface/formwork. This ensures that the sensor stays perpendicular to the main direction of thermal flux and has therefore a well-known position of measurement. Besides established sensors, novel techniques incorporating fibre optic sensors or thermographic methods for surface temperature monitoring have started to gain popularity.

9.3.2 Common Sensors and Their Peculiarities

9.3.2.1 Thermocouples

Thermocouples are commonly used sensors when it comes to in situ temperature monitoring of concrete, especially due to their comparably low cost, robustness and practicability (ASCE 2000).

The operating principle of the thermocouples is based on what has become known as the thermoelectric effect or "Seebeck effect" (discovered in 1821 by Thomas Johann Seebeck). In this phenomenon, voltage difference between two dissimilar electrical conductors or semiconductors is induced by temperature differences. This temperature-dependent voltage resulting from the thermoelectric effect is then interpreted to measure temperature (Morris and Langari 2016; Hagart-Alexander 2010).

There are different types of thermocouples, i.e. nickel alloy, platinum/rhodium alloy, tungsten/rhenium alloy, etc., and every particular type is denoted by a capital letter, i.e. Type E, Type K, Type T, Type R, etc., offering a variety of temperature ranges that can be measured and measurement accuracy (Tong 2001). The types which are commonly used in concrete temperature monitoring are Type K thermocouples (chromel–alumel) and Type T (copper–constantan) ensuring an accuracy of approximately 1.5–2 °C and 0.5–1 °C, respectively, which is adequate for the purpose of the measurement. Prior to the installation of the thermocouples, the ends of the two conductors have to be in direct contact which is usually accomplished by simply twisting them together or join them together through soldering or even welding (Omega Engineering 2000). A thermocouple connector is often required at the other end of the cable to enable connection between the thermocouple and the logger. An illustration of Type K and Type T thermocouples is shown in Fig. 9.13.

Once the thermocouples are prepared, the joined end of the wires is fixed to the desired locations, as exemplarily shown in Fig. 9.14.

(a) Type K thermocouple wire *(b) Type T thermocouple wire*

Fig. 9.13 Example of thermocouple wires (*Photographs* F. Kanavaris)

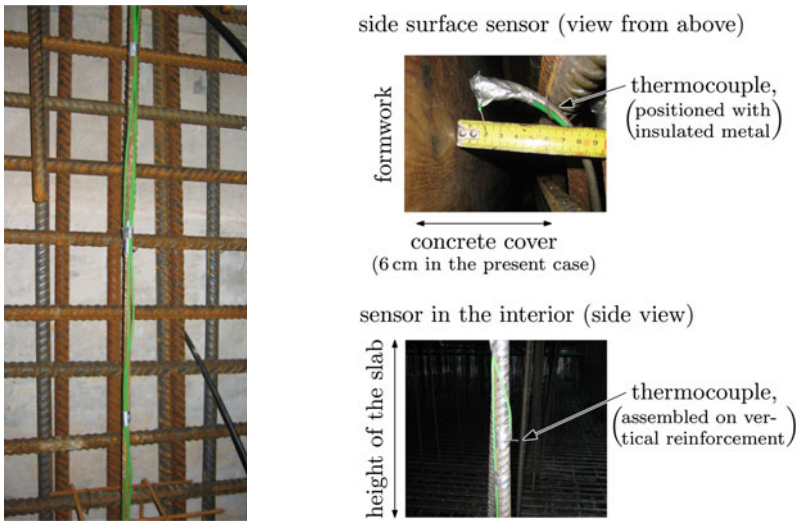

(a) Routing along the reinforcement *(b) Example of fixed measuring ends of thermocouples*

Fig. 9.14 Example of application of thermocouples in a concrete slab (*Photographs* D. Schlicke)

9.3.2.2 Resistance Temperature Detectors

Resistance temperature detectors (RTDs) are the temperature sensors which detect temperature through changes in resistance of a metallic material. The majority of RTD sensors are composed by a portion of fine wire wrapped around a ceramic or glass core, whilst the RTD wire is typically made of nickel, platinum or copper

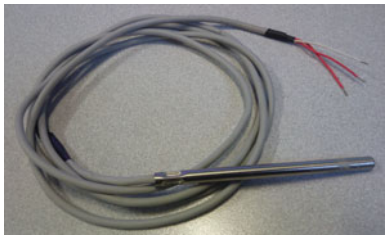

Fig. 9.15 Example of a commercially available RTD probe with PT100 (*Photograph* F. Kanavaris)

(Morris and Langari 2016; Hagart-Alexander 2010). In contrast to thermocouples, which measure temperature through changes in voltage, RTDs provide the higher accuracy, stability and repeatability. In detail, the accuracy of RTDs, such as PT100 (see Fig. 9.15), can be designed to fall below 0.2 °C.

Since RTDs operate at relatively low resistance, the influence of the lead wire resistance is not negligible (ASCE 2000). However, this is usually factored out by the manufacturer; otherwise, measurement distortions can occur. Although RTDs provide the highest measurement accuracy, they are generally among the most expensive temperature sensors.

9.3.2.3 Thermistors

Thermistors are electric resistors which also detect temperature through changes in resistance; however, thermistors differ from RTDs in terms of composing materials (Hagart-Alexander 2010) as well as their comparably high temperature coefficient of resistance (Nakra and Chaudhry 2016).

Thermistors are usually made of ceramic or polymer, whereby two principally different types of thermistors can be distinguished: PTC with positive temperature coefficient due to which resistance increases as temperature rises and NTC with negative temperature coefficient with decreasing resistance as temperature rises.

The high resistance coefficient contributes to measurement simplicity and minimization of potential errors arising from leading wires (ASCE 2000; Harris and Sabnis 1999), yielding slightly better accuracy than thermocouples, i.e. between 0.2 and 0.4 °C, whilst not being as cheap as the latter. An example of a pure thermistor as well as a ruggedized one specifically designed for measuring temperature of concrete is depicted in Fig. 9.16.

9.3.2.4 Sensing Along Optical Fibre Cables

Another opportunity of measuring temperatures is using optical fibre cable directly as sensing element by sensing along the cable length. So-called distributed temperature sensing systems (DTS) measure temperature along the optical sensor cable and provide a continuous temperature profile along the cable (e.g. Shi et al. 2016;

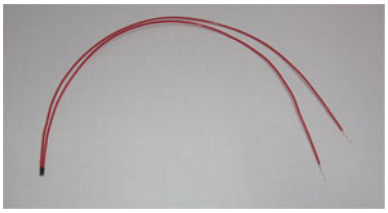

(a) "pure" thermistor (NTC)

(b) ruggedized thermistor placed with aramid sticks between reinforcement.

Fig. 9.16 Examples of thermistors (*Photographs* D. Schlicke)

Bao and Chen 2012; Ukil et al. 2011; Beck et al. 2010; Inaudi and Glisic 2006; Lee 2003). The provided accuracy of min. ±0.1 °C is sufficient for measurements in hardening concrete (Glisic and Inaudi 2007). The spatial resolution of such measurements, however, ranges commonly in the magnitude of decimetres (e.g. Glisic 2000; Lee 2003) and has been reported to be inversely proportional to the maximal distance range (Henault et al. 2011; Lee 2003).

9.3.2.5 Thermal Camera/Infrared Thermometers

Another technique for measuring the temperature history of hardening concrete that gains popularity is the infrared thermography or thermal imaging. With this technique, which has been previously used to detect defects in reinforced concrete (Milovanovic and Pecur 2016; Bagavathiappan et al. 2013), one can evaluate the surface temperature of objects using a thermal camera on the basis that all bodies emit thermal energy within the infrared wavelength band (Azenha et al. 2011; Childs 2001). The advantage of this method is that it can produce instantaneous real-time images (or videos) of the temperature distribution in the concrete surface, as well as its surroundings (Domski and Katzer 2015; Azenha et al. 2011; Weil 2004). Similarly to thermal cameras, infrared thermometers can be also used to provide an indication of the surface temperature of a concrete unit (Snell 2015); however, the spectrum of the infrared thermometers is narrowed down to a specific point and might not provide the capability of continuously recording the temperature. Additionally, some infrared thermometers also come with a thermocouple port enabling the simultaneous temperature measurement from the thermocouple and from the laser. One can fix several thermocouples in different locations of a mass concrete member and frequently evaluate the temperature differences between the concrete core and exposed surfaces for quality control purposes. An example of an image taken from a thermal camera and an infrared thermometer is shown in Fig. 9.17a and Fig. 9.17b, respectively.

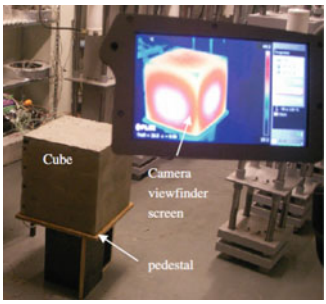

(a) Thermal image of concrete cube using a thermal camera (Azenha et al., 2011)

(b) Surface temperature measurement of a concrete slab with infrared thermometer (photo: F. Kanavaris)

Fig. 9.17 Examples of thermal camera and infrared thermometer

9.4 Monitoring of Strain Histories

9.4.1 Preliminary Remarks

Monitoring of strain history in mass concrete provides insights into the real deformation behaviour of the material. This includes concrete strains within the member but also the globally resulting deformation of the member. Next to further insights into the structural behaviour of hardening mass concrete, monitored strain histories provide also a strain-based opportunity to assess the resistance against cracking (Jung et al. 2017; Lawrence et al. 2014). In detail, this can be achieved by derivation of mechanical concrete strains out of the measurements (restrained part of thermal strains and shrinkage as well as additional viscoelastic strains) and their comparison with strain-based crack criteria. Of course, cracking itself would be determined directly by the measurement as soon as it occurs (Rostásy et al. 2007; Schlicke 2014).

With respect to strain monitoring in mass concrete, the literature review shows mainly the installation of so-called concrete embedment strain gauges as well as Carlson strain gauges. In general, concrete embedment strain gauges are characterized by an embeddable body which will deform together with the concrete and whose deformation is measured using different measuring principles. Usually, this procedure requires different post-processing, e.g. meaningful determination of the beginning of the monitoring (Azenha et al. 2009, 2014) and temperature compensation. In contrast to this, Carlson strain gauges combine different measuring principles in order to obtain the real concrete strain directly.

9.4.2 Common Measurement Equipment and Peculiarities

9.4.2.1 Electrical Resistance Strain Gauges

Electrical resistance strain gauges are sensors which measure induced deformation (strain) in a certain direction through a change in electric resistance and are used to detect relatively small displacements, i.e. 0–50 με (Morris and Langari 2016). Such sensors come at different sizes, where the selection of the appropriate size depends on the type of application and expected magnitude of strain (MM 2014a). These sensors are considered to be an efficient solution when it comes to strain monitoring in hardening concrete as they are relatively inexpensive, are available in different sizes and offer compatibility with numerous data loggers. Nonetheless, there are technical parameters that need to be taken into consideration when setting up a strain monitoring process, such as type of bridge (full, half and quarter), temperature compensation, gauge factor. More detailed information regarding the above is available in the existing literature (Nakra and Chaudhry 2016; Dally and Riley 2005; Harris and Sabnis 1999; Omega Engineering 1999).

The application of electrical resistance strain gauges in hardening mass concrete, however, is to be handled with caution because of their sensitivity to humidity as well as limited long-term stability (e.g. Rocha 1965). Bearing this in mind, two general types for application inside concrete have asserted: (i) electrical resistance strain gauges in specific devices for concrete embedment and (ii) electrical resistance strain gauges attached to reinforcement. With respect to monitoring of hardening mass concrete, specific examples were not obtained in the available literature. One reason for this could be found in the explanations of Azenha et al. (2009) indicating problems with the temperature compensation as well as vulnerabilities against interference with electrical apparatus in the sensors vicinity.

The second case, attaching the strain gauge on the reinforcement bars, is reported, e.g., in Kanavaris (2017), Faria et al. (2006), Bekowich (1968), Morabito (2001). Specific measures for providing an adequate steel surface in terms of smoothening and cleaning are required (e.g. Nakra and Chaudry 2016). The strain gauge is then adhered to the steel surface using a high strength glue/epoxy. It has to be noted that if the lead wires connected with the strain gauge are exposed, then they must not come in contact with the steel surface; otherwise, this will result in short-circuit occurrence. The protection of the strain gauge from water is then accomplished through application of a layer of a moisture protection coating in the strain gauge after it has been successfully attached to the desired location of the bar. Further information and details with respect to strain gauge installation can be found in MM (2014b, c, 2015). Finally, due to the fact the electrical resistance strain gauges are considerably sensitive and fragile sensors, protection against mechanical damaging, the gauge must be provided in order to ensure that the gauge will survive the rebar transportation (if the rebar is not in place) and concrete pouring process. Examples of the above processes are depicted in Fig. 9.18.

(a) strain gauge glued on smoothed steel re-bar

(b) moisture protection coating applied on strain gauge

(c) strain gauge protected against mechanical damage

Fig. 9.18 Example of strain gauge installation on a steel rebar (Kanavaris 2017)

Although it becomes rather obvious, it has to be pointed out that the strain measured from attaching strain gauges on the reinforcement bars is not the real strain induced in concrete. Apart from this, since the reinforcement ratio is kept relatively low in mass concrete applications and the reinforcement is predominately concentrated close to concrete surfaces, assessment of the strains in concrete core requires the application of additional reinforcement bars. Besides, such measurement is affected by a disproportionate slip between young concrete and reinforcement until concrete is stiff enough to ensure bonded deformations to steel. Up to such instant, which is difficult to ascertain, the measurements taken by strain gauges glued into reinforcement cannot be considered as representative of concrete deformations (Azenha et al. 2014).

9.4.2.2 Vibrating Wire Sensor

The application of vibrating wires in hardening mass concrete has a considerable history going back several decades (e.g. Mainstone 1953; Rocha 1965; Geymayer 1967). Nowadays, vibrating wires can be seen as the most established type of concrete embedment strain gauges (Jung et al. 2017; Lawrence et al. 2012, 2014; Yeon et al. 2013; Chu et al. 2013; Choi and Won 2010; Azenha et al. 2009, 2014, 2017; Zreiki et al. 2010; Sellers 2003; Morabito 2001 and Heimdal et al. 2001a, b). These sensors usually consist of a wire and a coil within a pipe which spans between two head plates. The basic measurement principle is the acquisition of the vibrating resonance frequency of the wire when excited by the coil. Due to the embedment in the concrete, the head plates will move apart or to each other when the concrete deforms, and by this the force in the wire changes. The according change of the vibrating resonance frequency of the wire enables to infer on the deformation of the concrete. For illustrative purposes, Fig. 9.19 shows an example

(a) "pure" vibrating wire sensor according to (Geokon, 2017)

(b) vibrating wire sensor applied in the reinforcement layer (photo: D. Schlicke)

Fig. 9.19 Vibrating wire sensor for embedment in concrete

of a pure vibrating wire sensor as well as its application on-site for measuring concrete strain within the reinforcement layer.

In general, vibrating wires record any real deformation along the measuring length, e.g. unrestrained thermal deformation, unrestrained shrinkage and creep (unrestrained viscoelastic behaviour).

However, vibrating wires require temperature compensation procedures that strictly depend on the coefficient of thermal dilation of the wire placed internally, which is constant and known (Azenha 2009). The temperature change in the measuring point is generally simultaneously monitored with a built-in thermistor inside the gauge body of vibrating wire sensors. Altogether, the real deformation in the measuring point can be derived from the vibrating wire measurement by:

$$\Delta\varepsilon_{\text{real}} = \Delta\varepsilon_{\text{meas}} + CTE_{\text{W}} \cdot \Delta T \tag{9.1}$$

where:

$\Delta\varepsilon_{\text{real}}$ Real strain in the measuring point,
$\Delta\varepsilon_{\text{meas}}$ Uncompensated recorded strain in the measuring point,
CTE_{W} Coefficient of thermal dilation of the wire,
ΔT Temperature change in the measuring point.

For profound understanding of the basic functionality of a vibrating wire, Fig. 9.20 illustrates the relation between concrete strain and wire deformation with respect to thermal dilation and shrinkage under different restraint situations. Besides, the effect of different coefficients of thermal dilation of the wire (CTE_{W}) and the concrete (CTE_{c}) is regarded as well.

In unrestrained conditions, the uncompensated strain of the vibrating wire corresponds to shrinkage as well as the difference in thermal dilation of wire and concrete. In restrained conditions, however, the vibrating wire displays the restrained part of thermal dilation of the concrete plus the difference in thermal dilation of wire and concrete as well as the unrestrained parts of shrinkage and viscoelastic strains. With respect to viscoelastic behaviour of concrete, it should be emphasized again that the vibrating wire records only unrestrained deformation so that restrained viscoelastic strains (recognizable as relaxation) are not recorded.

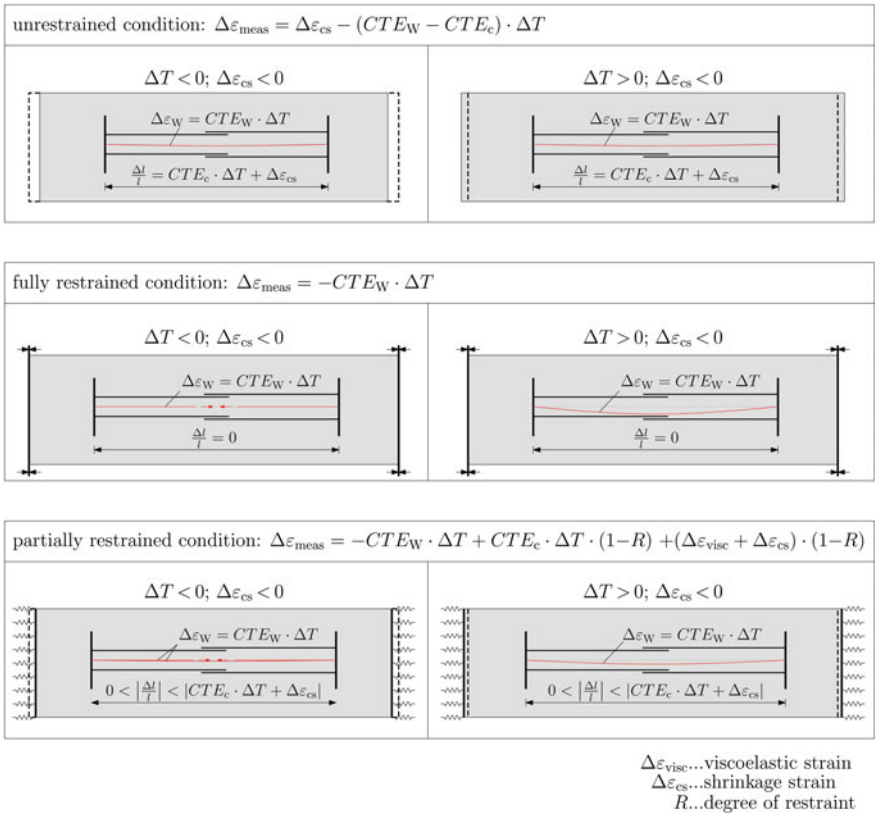

Fig. 9.20 General functionality of vibrating wire according to Schlicke (2014)

9.4.2.3 Concrete Embedment Strain Gauge on Basis of Fibre Optic Sensors

The application of concrete embedment strain gauges on basis of fibre optic sensors (explicit fibre optic sensor connected and controlled with a fibre optic cable), however, increases recently, especially in case of comprehensive programmes in which additional costs of the optical measuring device (interrogator) can be amortized by a considerable reduction of cabling efforts due to the serial connectivity of fibre optical sensors. Such sensors work on basis of fibre Bragg technique with a specific Bragg grating of the fibre in the measuring length. Similarly to vibrating wires, these sensors record an average strain in the measuring length. Figure 9.21 shows such a sensor.

Fig. 9.21 Fibre optical concrete embedment strain gauge on basis of fibre Bragg technique (*Photograph* D. Schlicke)

9.4.2.4 Carlson Type Strain Gauge

One of the most widely used sensors to monitor internal strains of mass concrete structures is the Carlson type strain gauge (Bekowich 1968; Nagataki 1970; Poblete et al. 1988; Shahawy and Arockiasamy 1996; Myrvoll et al. 2003; Conceição et al. 2014). This sensor contains a set of electrical strain gauges. The sensing element of Carlson type strain gauge includes two coils of carbon steel wire (elastic material), one of which increases in length and consequently in electrical resistance when a strain occurs, whilst the other decreases. One important aspect is that the ratio of the two registered resistances is independent of temperature and, therefore, the change in resistance ratio can be used to indicate strain. Besides that, the total resistance is independent of strain since one coil increases the same amount as the other decreases due to the change in length of the sensor. Hence, the total resistance can therefore be used to indicate temperature. This is one of the main advantages of using Carlson type strain gauges: the same instrument is capable to make both strain and temperature measurements, allowing the reduction of temperature sensors in the structure and the number of channels required for the data acquisition system. Further details on Carlson type strain gauges are given in Torrent and Fucaraccio (1982).

Carlson type strain gauges' body is usually shaped like a cylinder with a metallic flange at either extremity. The cylinder cover is usually made with PVC sleeving to break the bond with the concrete. The role of these flanges is to promote the bonding to the surrounding concrete. The PVC cover has a hollow section with the steel rods connected to either end. The elastic wire coils are mounted on these rods such that when the end flanges are pulled apart, one coil increases in length whilst the other decreases. The coils of steel wire are immersed in oil; the housing is hermetically sealed. This procedure results in a strain gauge with good stability and reliability. A schematic representation and a picture of Carlson strain gauges and application examples are shown in Fig. 9.22.

In the same way as with strain gauges on basis of electrical resistance, Carlson strain gauges are usually connected to a measuring three-wire, quarter-bridge wiring scheme in order to minimize cable effects (Myrvoll et al. 2003).

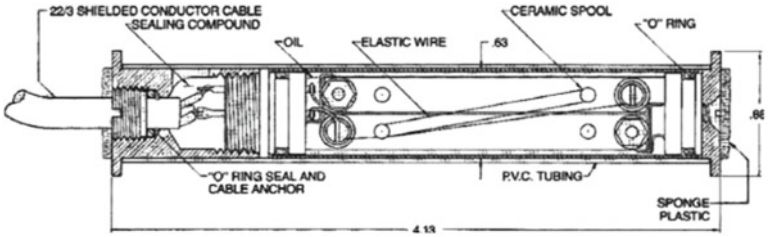

(a) Scheme of Carlson strain gauge taken from Myrvoll (2003)

(b) Carlson strain gauge (RST Instruments 2017)

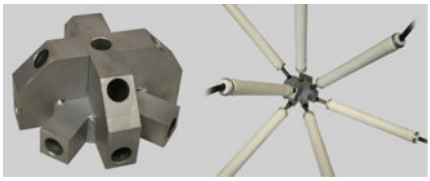

(c) Spider and Carlson strain gauges shown in a spider (RST Instruments 2017)

(d) Carlson strain gauges being grouped by a spider (Mata et al. 2015)

Fig. 9.22 Carlson type strain gauge and application opportunities

The installation procedure of Carlson type strain gauges requires a previous calibration in situ. This procedure is usually performed using a calibration device, e.g. micrometre screw or other displacement transducer.

9.4.2.5 Sensing of Concrete Strains with an Optical Fibre Cable Directly

This section refers to strain monitoring using the optical fibre cable directly as sensing element. In detail, two different methods can be distinguished: (i) fibres with fibre Bragg grating (FBG) and (ii) continuous sensing along the fibre without FBG. Regarding the general functioning of this technique, reference is made to Rogers (1999), Hill and Meltz (1997), Lee (2003), Henault (2013), Billon et al. (2014) or Delepine-Lesoille et al. (2017).

One of the main challenges of applying this technique to hardening concrete is the protection of the fibre and ensuring at the same time a meaningful connection between fibre and concrete (Delepine-Lesoille et al. 2006). The pure fibre is usually

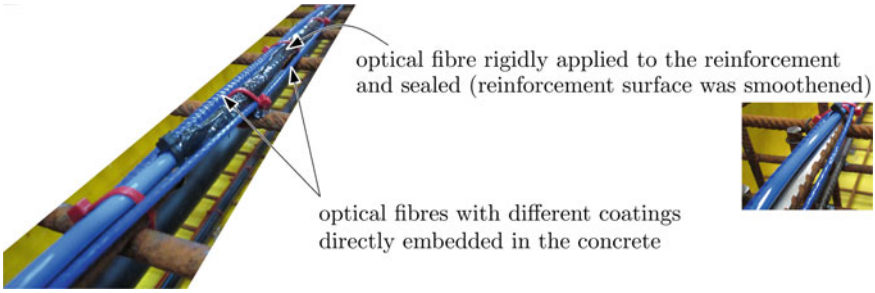

Fig. 9.23 Sensing of concrete strains with optical fibre cables directly (*Photograph* D. Schlicke)

too fragile to survive the pouring. But a helpful protection coating is also to be seen critical since it is expected to be too weak and thus the strain of the fibre is only presenting the smeared concrete strain over an undefined length. A ruggedized fibre optical sensor developed in EPFL known as SOFO has been also used in several monitoring programmes reportedly offering resolution in the micrometre range, long-term stability and insensitivity to temperature (Glisic and Inaudi 2007; Glisic and Simon 2000). Recent activities concentrate on application of the fibre on specifically prepared reinforcement surface but as mentioned before, this refers to a measurement of steel strain changes and requires again additional assumptions to draw conclusions on the real concrete strain. Figure 9.23 depicts different fibre applications for a comparative study; however, a report on these particular measurements was not available at this time.

Another challenge is the required strain resolution. Different specifications can be found in the literature indicating a resolution of *a few micrometres over one metre* (Bao and Chen 2012) up to 20 µm/m (Lee 2003) and higher. The required resolution for strain monitoring in hardening concrete ranges in the same order of magnitude. For example, the depicted strain monitoring of power plant slab Boxberg showed a real deformation to be monitored in the cooling phase of ca. −150 µm/m within ∼840 h, whereby the desired resolution for monitoring the strain evolution over time would range in the magnitude of ±3 µm/m per time step.

In case of cracking, the absolute size of strains increases locally in the surrounding of the crack; however, the associated increase of inhomogeneity of the strain field influences the measurement signal considerably. But at the same time, the local disturbance enables also the recognition of crack formation at a very early stage, even before cracks would be visible (Lee 2003; Bao and Chen 2012).

9.4.3 Experiences and Observations from Application

Nowadays, the most established technique is the embedment of 15–20-cm-long concrete embedment strain gauges in measuring direction (Jung et al. 2017;

Lawrence et al. 2012, 2014; Yeon et al. 2013; Chu et al. 2013; Choi and Won 2010; Azenha et al. 2009, 2014, 2017; Zreiki et al. 2010; Sellers 2003). The required accuracy can be obtained independently from the measurement principle, e.g. vibrating wire-based, electrical strain gauge-based or fibre optic-based devices.

The application of Carlson type strain gauges, however, is declining (ASCE 2000). Vibrating wire and fibre optic-based sensors have largely superseded the Carlson type strain gauge because their signals can be transmitted over long cables without degradation with relative immunity to changes of cable or contact resistance. In addition, the vibrating wire and fibre optic-based strain gauges have excellent long-term stability.

9.5 Determination of Stress Histories

9.5.1 Preliminary Remarks

The determination of stress histories in mass concrete on basis of measurements provides insights into the real stressing in a material point and enables the assessment of resistance against cracking by comparison of the determined stresses with stress-based crack criteria. Of course, cracking itself would be determined directly by the measurement as soon as it occurs (Rostásy et al. 2007; Schlicke 2014). With respect to the reports in the literature, three basic procedures can be distinguished:

1. Computational derivation of stresses from pure strain measurements,
2. Application of "no-stress" enclosures for simplification of the analysis of pure strain measurements and
3. Determination of stresses with specific measuring devices.

The computational derivation of stresses from pure strain measurements can be achieved by a clear identification of all stress-relevant parts in the strain measurement and superimposing them with the evolution Young's modulus.

The application of "no-stress" enclosures can be seen as a supporting measure in order to simplify the identification of stress-relevant parts in the strain measurement; however, this solution still requires computational post-processing since the effects of viscoelasticity and evolution of Young's modulus are not included.

The determination of stresses with specific measuring devices basically refers to an exclusive measurement of all stress-relevant concrete strains so that the measured values can provide a good estimate on concrete stresses without the need of advanced post-processing as in the previous solutions. But this method should not be misinterpreted as a direct stress measurement since its basic measurement principle is usually also deformation-based (strain gauge in a load cell).

9.5.2 Derivation of Stresses from Pure Strain Measurements

Pure strain measurements in hardening mass concrete are significantly influenced by the present degree of restraint. The results consist of either restrained or unrestrained parts of thermal strains (depending on the measurement principle) as well as of unrestrained parts of shrinkage and viscoelastic strains in form of creep.

For the derivation of stresses from such results, several approaches can be found in the literature. These approaches basically differ in terms of time discretization and consideration of viscoelasticity (e.g. Richardson 1959; Yeon et al. 2013; Bazant 1972a, b; Acerbis et al. 2011; Choi et al. 2011 or Schlicke 2014).

Solutions with implicit consideration of viscoelastic strains by modification of Young's modulus, the so-called effective modulus method, are user-friendly and well-established in practice (Bazant 1972b). In detail, these approaches consider viscoelasticity by multiplication of stress-independent strains with an accordingly modified Young's modulus, so that the stress response includes viscoelastic effects. However, the implementation of such approaches in time step-based solutions should be seen critical since they can require factitious modifications in unloading phases within the stress history or at later ages with very small changes of the stress-independent strains (e.g. Tue et al. 2007; Nietner et al. 2011).

A desirable solution with respect to mechanical consistency is a time discrete approach with explicit consideration of shrinkage and viscoelasticity in the course of time. Given the case that the strain measurement consists solely of the real concrete strains, the general solution would hold:

$$\sigma_c(t) = \int_{t_0}^{t} [\Delta\varepsilon_{real}(t) - \Delta\varepsilon_{ct}(t) - \Delta\varepsilon_{cs}(t) - \Delta\varepsilon_{cc}(t)] \cdot E_c(t)\mathrm{d}t \tag{9.2}$$

where:

$\sigma_c(t)$ Stress history in the measuring point,
$\Delta\varepsilon_{real}(t)$ History of real strain increments in the measuring point (here it is assumed that the measurement result consists solely of the unrestrained parts of thermal strains, shrinkage and viscoelastic strains),
$\Delta\varepsilon_{ct}(t)$ History of temperature strain increments in the measuring point,
$\Delta\varepsilon_{cs}(t)$ History of total shrinkage strain increments in the measuring point,
$\Delta\varepsilon_{cc}(t)$ History of total viscoelastic strain increments in the measuring point,
$E_c(t)$ Evolution of Young's modulus.

9.5.3 Derivation of Stress History with Strain Gauges in "No-Stress" Enclosures

A technique used to measure and compensate for shrinkage and thermal strains from the total or apparent strain measured by the sensors is the use of strain gauges

in "no-stress" enclosures (Rocha 1965; Choi et al. 2011; Chu et al. 2013; Yeon et al. 2013; Azenha et al. 2014). The "no-stress"-induced strain gauges are "dummy" strain gauges that are installed in a manner which isolates them from the effects of stress changes but under the same environment as the active strain gauges. Thus, this "dummy" sensor is subjected to the same history of temperature and humidity (if the enclosure is porous) suffered by the other strain gauges, being able to respond to and measure the unrestrained volume change of surrounding concrete.

In practice, the "no-stress" strain gauge consists of one regular concrete embedment strain gauge, e.g. electrical resistance, Carlson type, vibrating wire or fibre optic-based, that is embedded in a cylinder of concrete which is set in a foam-padded box (Figs. 9.24 and 9.25). The foam is attached to alleviate the friction between the concrete and the inner surface of box and to allow the volume changes of concrete inside the box without restraints, ensuring a stress-free condition in concrete. This box is filled with the same concrete, and at the same time the concrete of monitored structure around it is poured. Then, the box is installed inside the concrete structure, near the other active strain gauges.

The enclosure box to install the strain gauge is generally provided by the concrete embedment strain gauges' manufacturers (e.g. Geokon 2017; RST Instruments 2017). Nonetheless, some works have already reported the successful use of handmade produced enclosures to obtain the "no-stress" strain gauge (Yeon et al. 2013; Azenha et al. 2014).

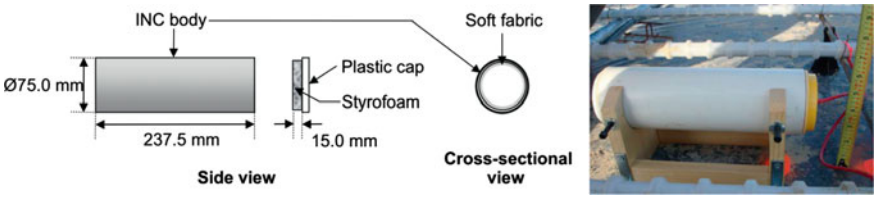

Fig. 9.24 Scheme and photograph of the enclosure used by Yeon et al. (2013)

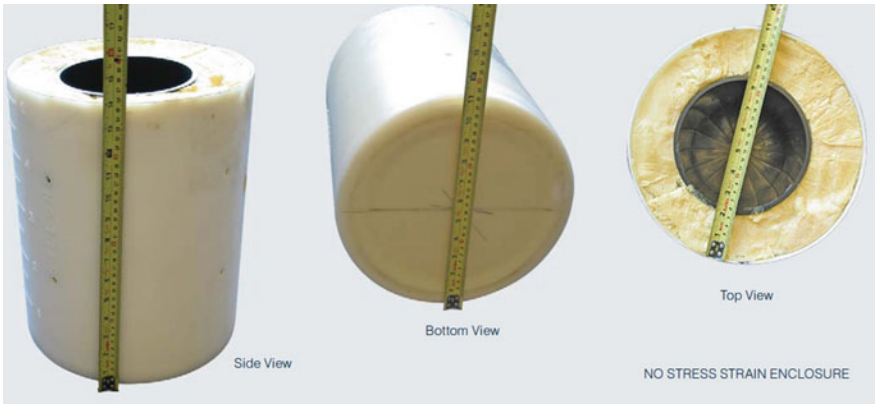

Fig. 9.25 Details of "No-stress" strain enclosure provided by RST Instruments (2017)

The stress history can be derived using Eq. 9.2, considering that the measurement made by the "no-stress" strain gauge corresponds to stress-independent parcel of the total measured strain. Thus, the measurement registered by the "no-stress" strain gauge represents the sum of terms $\Delta\varepsilon_{cs}(t)$ and $\Delta\varepsilon_{ct}(t)$ that stands for, respectively, the increment of the unrestrained shrinkage (autogenous and, possibly, drying shrinkages) and thermal strains between the time $t - 1$ and t.

9.5.4 *Determination of Stresses with Specific Measuring Devices*

As aforementioned, the determination of stresses with specific measuring devices aims at the measurement of concrete stresses without the need of any post-processing. A basic requirement of this technique is to provide thinnest possible sensors in order to reduce factitious stress concentrations in the vicinity of the sensor (Rocha 1965; Raphael and Carlson 1965; Carlson 1966). According to this requirement, a very flat sensor connected with a Carlson strain gauge, a so-called Carlson stressmeter, was developed and applied in several dam projects in the early second half of the last century. One mandatory requirement of these sensors was the application on a stiff surface which led to primary applications in construction joints.

With respect to recent reports in the literature, the more established technique of today appears to be a longer rod-shaped device encapsulating a cylinder of concrete within the poured concrete and coupling this in series with a load cell (e.g. Kawaguschi and Nakane 1996; Tanabe 1998; Rostásy et al. 2007; Tue et al. 2007, 2009; Kurata et al. 2009; Choi and Oh 2010; Choi et al. 2011; Schlicke 2014, 2015). The load cell is also thin; however, the encapsulated cylinder enables the installation of the sensor away from the construction joint and at the same time, the comparably equal properties of the concrete in the tube ensure a suitable consideration of evolution of Young's modulus. Figure 9.26 shows a scheme of the Geokon stressmeter based on Geokon (2015).

In the shown solution of Fig. 9.26, the concrete cylinder is approximately 0.5 m long and has a diameter of ca. 6.5 cm. Its encapsulation is achieved by a permeable tube which ensures the same concrete properties inside the tube as in the surrounding of it. At the same time, this encapsulation allows the concrete cylinder to interact with the stiffness of the load cell in the longitudinal direction of the sensor.

The orientation of the sensor controls the direction of stresses to be monitored. Another important detail of this measuring principle is the prevention of friction on the inside of the tube by a very smooth surface.

Sufficient filling of the tube and compacting of the concrete inside is achieved by the following procedure: (1) taking sensor out of its final position when the pouring process reaches this level, (2) filling the tube with the same fresh concrete, (3) compacting and closing the tube, (4) assembling the sensor in the final position and (5) setting in concrete by continuation of pouring. Figure 9.27 illustrates this procedure.

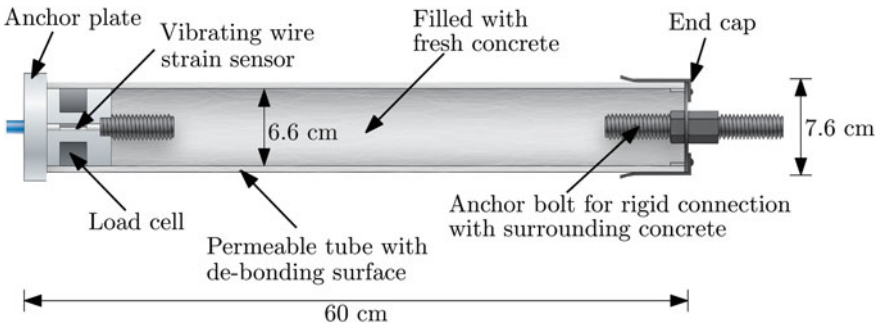

Fig. 9.26 Scheme of Geokon stressmeter, according to Geokon (2015)

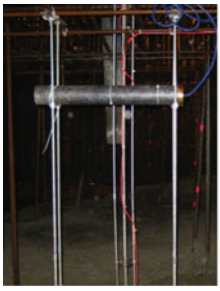

(a) preparation of stressmeter application before casting

(b) filling and compacting of the tube with fresh concrete when casting reaches the measurement point

(c) final application of the filled and closed stressmeter and continuation of casting

Fig. 9.27 Application of stressmeter (*Photographs* D. Schlicke)

The stress in the surrounding concrete can finally be derived from the recorded load divided by the cross-sectional area of the encapsulated cylinder. Typical, results are shown in Fig. 9.9.

9.6 Selected Application Examples

9.6.1 Wall of the Entrance of Paradela's Dam Spillway

Between the years of 2010 and 2012, a new spillway was built for the Paradela's dam, Portugal. A part of this building is a thick wall that pertains to the entrance of the dam spillway. The wall is 27.5 m long, with a maximum width of 2.8 m and height of 15.0 m. The constructors and owners were worried about a construction

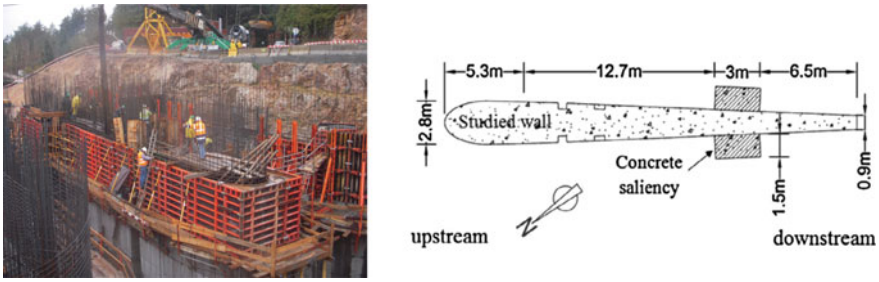

Fig. 9.28 Wall of entrance of Paradela's dam spillway: construction phase studied (*Photograph* M. Azenha; *Drawing* Azenha et al. 2014)

phase in which a 2.5-m-tall batch was poured (total of 150 m^3 of concrete); see Fig. 9.28.

Because of the thermal crack risk involved, an in-depth consulting work was contracted so that the cracking risk was assessed. The study encompassed laboratory thermal and mechanical characterization of concrete, thermomechanical simulation with finite element method as well as in situ monitoring of temperatures and strains. The solution implemented to control the temperature elevation and, consequently, high stresses in the structure was the use of a post-cooling system based on the used air-cooled prestressing ducts placed longitudinally along the wall. Details about this case study can be found elsewhere (Costa 2011; Azenha et al. 2014).

The monitoring programme has been carried out in situ to better understand the effectiveness of the cooling system, its influence on the cracking risk and assess the capabilities of the adopted numerical simulation strategy. The programme involved the use of 27 temperature sensors (20 Type K thermocouples and 7 resistive temperature sensors) and 7 vibrating wire strain gauges embedded in concrete. Particular attention was given to the evaluation of the effectiveness of the cooling system, with temperatures being measured at several points along the prestressing ducts, and with air velocity measurements taken with hand-held anemometers. Figure 9.29. illustrates the internal temperature and strain measuring points.

The sensors were positioned aiming particularly at assessing temperature profiles in a region near the maximum width of the wall. The placement of sensors in this section is depicted in the scheme of Fig. 9.29a, where thermocouples are identified by the prefix TC and vibrating wires and resistive temperature sensors are labelled as VW. The internal air temperature of prestressing ducts has been monitored in the same section and in neighbouring areas. Environmental temperature (dry-bulb) has been also assessed with a thermocouple.

Monitoring was carried out since the instant of casting during a period of 10 days, and the measurement frequency was set to 1 reading per each 30 min. The internally monitored temperatures in concrete are shown in Fig. 9.30 for a vertical and a horizontal alignment of sensors that passes through sensor VW3. From this figure, it can be seen that the initial temperature of concrete was $\sim$ 15 °C and the

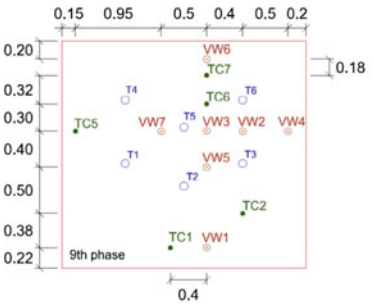

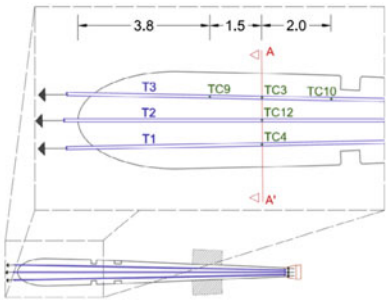

(a) measuring points (TC: thermocouples; VW: resistive thermistors and vibrating wire strain gauges; T1 to T6: air cooled prestressing ducts, units: m)

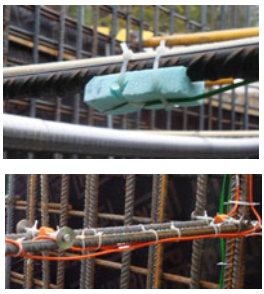

(b) detail of type K thermocouples and vibrating wire strain gauges

(c) detail of "no-stress" strain enclosure

Fig. 9.29 Monitoring programme in a wall of Paradela's dam spillway (*Drawings* Azenha et al. 2014; *Photographs* R. Lameiras)

peak temperature was approximately 42 °C in the core regions (VW3 and VW5). Furthermore, it can be observed that the ascending branch of temperature development is clearly affected at the age of 14 h, when the cooling system is activated. In specific regard to the vertical profile of temperatures shown in Fig. 9.30, the expectable behaviour was captured: the core region has the highest peak temperatures (VW3, VW5), whereas a decreasing trend is seen towards the top surface. In fact, sensors TC6 and TC7 exhibit maximum temperatures of ∼36 °C, whilst VW6 (near the top surface) has the lowest peak temperature (∼27 °C). Near the bottom surface of this construction phase, sensor VW1 highlights the importance of the heat storage effect caused by the previously cast concrete: in fact, even though the temperature peak is lower than that of the core regions, it occurs later and the heat loss rate observed afterwards is lower than in other regions. It should also be remarked that all sensors are almost in equilibrium with environmental temperature by the age of 8 days.

Strain measurement was carried out with vibrating wire strain gauges of metallic casing with 14 cm reference length. The strain gauges were placed at the locations

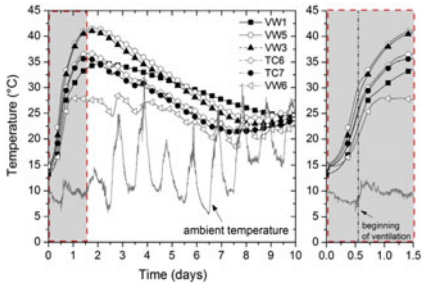

(a) monitored temperatures – vertical alignment

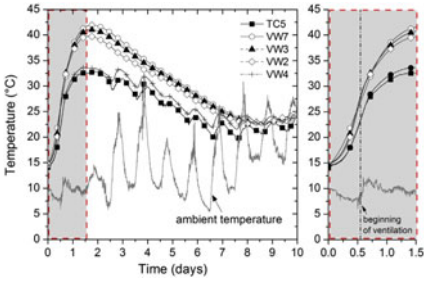

(b) monitored temperatures – horizontal alignment

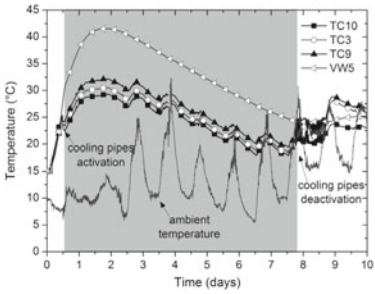

(c) temperature profile along the prestressing duct

Fig. 9.30 Temperature results in the monitored construction phase of Paradela's dam spillway (Azenha et al. 2014)

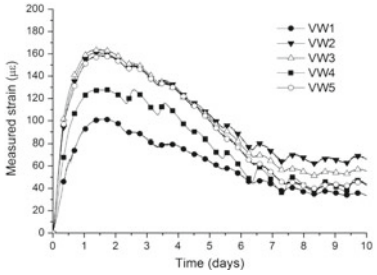

(a) measured strains

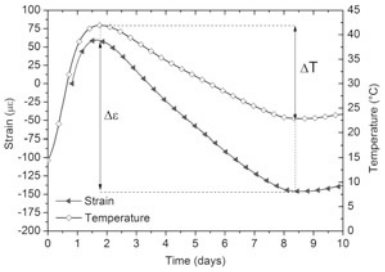

(b) temperature and strains in the "no stress" enclosure

Fig. 9.31 Strain results in the monitored construction phase of Paradela's dam spillway (Azenha et al. 2014)

dully positioned in order to measure strains in the longitudinal direction of the wall. Measurements were taken with the same data logger and at the same sampling rate as it was the case for temperature sensors. The measured strains in sensors VW1 to VW5 are shown in Fig. 9.31a.

In order to assess free deformations of the concrete used in the construction (associated with unrestrained autogenous shrinkage and thermal deformations), strain was measured in a "no-stress" enclosure at position VW 7. The concrete cylinder in this "no-stress" enclosure had dimensions of 150 mm diameter and 300 mm length and was prepared simultaneously with the studied construction phase. In detail, the concrete was cast into the mould right before the casting progress reached the location VW7 and then the mould was placed horizontally at the targeted position before continuing and finishing of the casting.

Reliable results were obtained by using the same concrete and a special mould which was internally coated with a soft membrane (with lids also coated with such material). The longitudinal strains in this specimen were measured with a strain gauge inside the mould, as shown in the photograph of the open mould in Fig. 9.29c. The results are given in Fig. 9.31b. Unfortunately, due to undetermined causes, the output of the sensor could not be read during the first 0.8 days, and thus the reported data only starts at such age.

9.6.2 Ground Slab Boxberg

The ground slab Boxberg is a 3.80-m-thick slab for a coal-fired power plant in Germany. It has aerial dimensions of $\sim 100 \times 100$ m and was poured in 5 construction stages. One construction stage with $\sim 10{,}000$ m^3 was comprehensively equipped with temperature sensors, vibrating wires and stressmeters in order to quantify the hardening-induced stress history of this construction stage. Measurements were carried out at two locations in this construction stage with ~ 15 sensors over the height at each location. Figure 9.32 illustrates the monitoring programme. Details about this case study can be found elsewhere (Tue et al. 2009; Schlicke 2014, 2015).

The following explanations concentrate on the measurement results and derived conclusions for the measuring location in the inner part of the slab. As illustrated in Fig. 9.33a, the measuring results at this location can be characterized by:

- Significant temperature differences over the height of the cross section,
- Significant stress differences over the height of the cross section and
- Absolutely shifted but parallel to each other running deformations.

As illustrated in Fig. 9.33b, the analysis of these results with respect to the characteristic parts in the cross section shows:

For temperatures:

- High uniformly distributed temperature field changes over time (ΔT_N) and

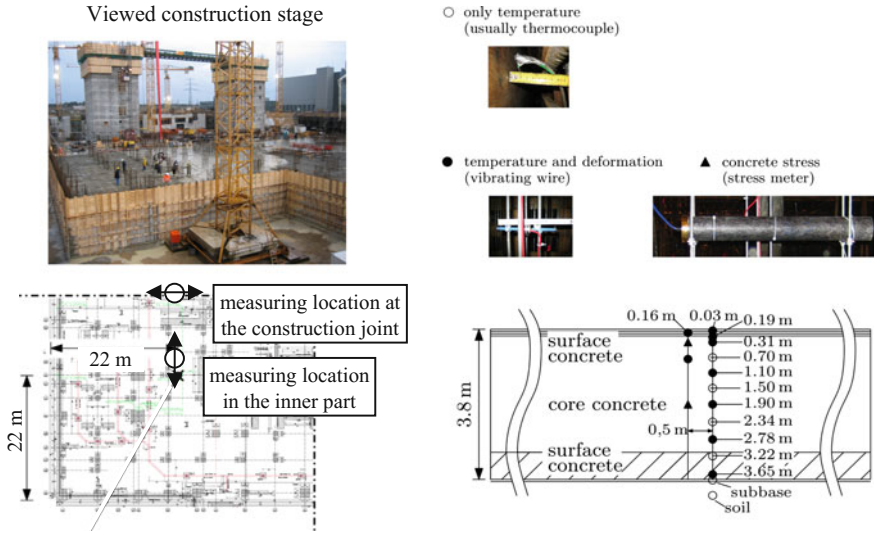

(a) construction stage and position of measuring points and measuring direction

(b) sensors arrangement over the height in a measuring point

Fig. 9.32 Monitoring programme ground slab Boxberg, measuring point "inner part of the slab" (*Photographs* D. Schlicke; *Drawings* Schlicke 2014)

- A high temperature gradient ΔT_M at very early ages resulting from an accelerated warming of the upper layers during the construction process meanwhile the bottom layer is still influenced by heat loss to the ground;

For stresses:

- Disproportional small centric restraint,
- Disappearing bending restraint at time of temperature equalization (bending is only significant during the construction progress) and
- Considerable eigenstresses;

For deformations:

- Almost congruent results at bottom, in the core and on top if the temporal offset due to retarded construction process with layers is considered.

The results of these observations are very consistent and can even be verified by themselves. Namely:

- The free deformation of all measuring points over the height reaches almost $\alpha_T \cdot \Delta T_N$ which confirms the very small centric restraint.

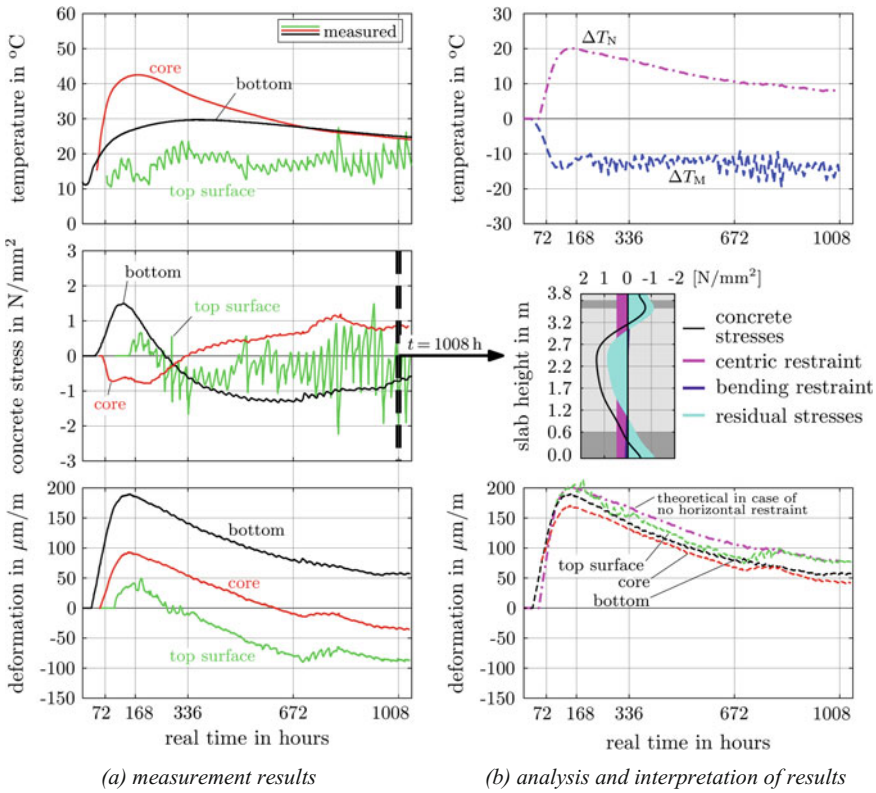

Fig. 9.33 Monitoring results for measuring point in the inner part of the construction stage (Schlicke 2015)

- The free deformation of all measuring points over the height shows almost no curvature which confirms the results of bending restraint.
- The free deformation of all measuring points over the height indicates an almost even cross section which confirms the almost perfect restraint of nonlinear parts of $\Delta T(z)$ causing the determined eigenstresses.

The above shown stresses were computationally derived from the strain measurements with vibrating wires. The reliability of their determination was verified by the compatibility check against the results of a stressmeter measurement in specific points of the cross section. In particular, stressmeters were positioned redundantly next to the vibrating wires at two selected heights of each measuring point (on half height as well as in the upper part of the slab, as shown in Fig. 9.32).

The results of the compatibility check on half height of the slab were already given in Fig. 9.9 for illustrative purpose of the compatibility check in general. Altogether, the compatibility check was considered as successful in the present case since the monitored stress history could be retraced quantitatively over the course of

time from the monitored strain history. Of course, this compatibility check refers rather to a verification of the material model than to a verification of the measurement technique itself. But with respect to a limited number of possible stressmeters in a cross section, a verification of the material model provides an appropriate basis for the derivation of stress histories in other points of the cross section.

In case of the monitoring programme ground slab Boxberg, the most important conclusion was the derivation of reasonable assumptions for efficient minimum reinforcement design of massive ground slabs, namely:

- Centric restraint can be neglected meanwhile.
- Bending restraint has to be taken into account.

Further results and conclusions of this monitoring programme as well as of similar monitoring of other member types are given in Schlicke (2014).

9.6.3 VeRCoRS (Focus on Fibre Optics)

VeRCoRs is a comprehensive project co-ordinated by Électricité de France (EDF) in which a mock-up of a reactor containment building was constructed with comprehensive monitoring of both early age as well as long-term behaviour. The mock-up, which is shown in its almost final stage in Fig. 9.34, consists of double

Fig. 9.34 VeRCoRS mock-up of a reactor containment building (Corbin and Garcia 2016)

containment walls made of reinforced concrete with a thickness varying between 0.7 m at the bottom of the inner wall and 0.4 m at the top of both containment walls.

More than 500 sensors were installed in the building in order to enable continuous monitoring of the behaviour of concrete, including temperature and humidity sensors, electrical resistance and vibrating wire strain gauges as well as 2 km of fibre optic cable sensors. With respect to the overall context of the present report, the following section concentrates on the monitoring of temperature and strain development in the hardening phase of the first lift of the inner wall, i.e. the "gusset", with a comparably thick cross-sectional dimension of 0.7 and 0.4 m thick and 1.20 m high.

Focus will be given on the application of innovative fibre optic techniques for the recording of temperature and strain development in the hardening concrete. In the present case, the fibre optic cables were placed across the circumference of the inner containment wall, as shown in Fig. 9.35b, measuring temperature and strain on an hourly basis.

The installation of fibre optic sensors under construction site conditions requires special care, especially to secure the cables during the pouring process. Reportedly, 80% of the fibre optic sensors survived the concrete pouring process, underlining the sensitivity of this type of sensor. Figure 9.36 gives an optical impression of the installation.

The advantage of the continuous measurement of temperature and strain using fibre optic sensors in the nuclear containment building is also shown in Beck et al. (2016), where sensor positioning and obtained strain histories across the circumference of the structure are demonstrated. The potential of obtaining continuous real-time measurements of temperature and strain evolution over considerably long distances undoubtedly contributes to a more comprehensive monitoring of mass concrete behaviour.

(a) sensor and their cables distributed in the circumference of the vessel

(b) fibre optic cable sensor running parallel to the reinforcement

Fig. 9.35 Monitoring sensors in the VeRCoRs project (Oukhemanou 2016)

(a) fibre optic cable sensors secured in place and grouped together

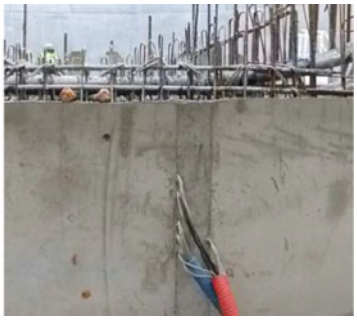

(b) residual sensor cables after concrete pouring and hardening

Fig. 9.36 Fibre optic sensors installed in the VeRCoRs project (Oukhemanou 2016; Oukhemanou et al. 2016)

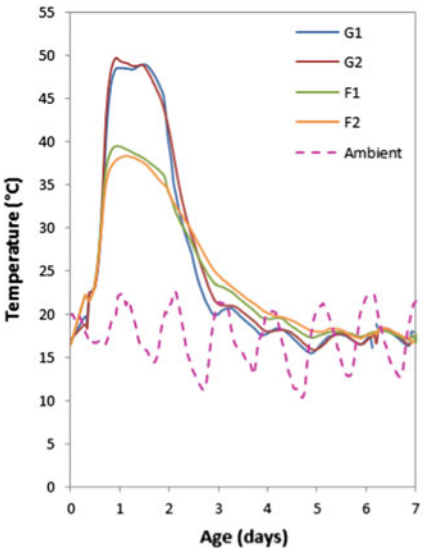

(a) Recorded temperatures in various locations in the "gusset"

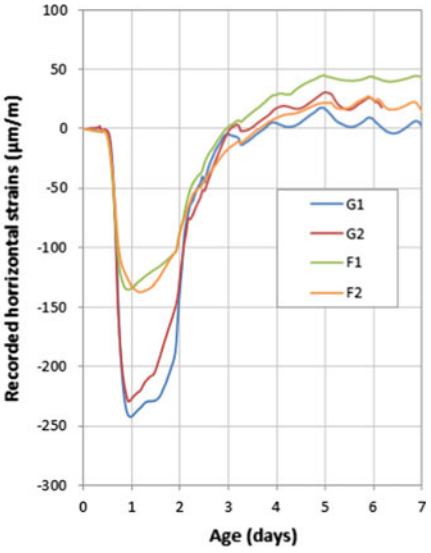

(b) Recorded horizontal strain histories in various locations in the "gusset"

Fig. 9.37 Example of results obtained from early-age monitoring in VeRCoRs project ("gusset"), adopted from Corbin and Garcia (2016)

Temperature and strain profiles obtained, see Fig. 9.37, are particularly useful in validating developed models in a more global manner (Kanavaris et al. 2016) and evaluating the effect of discontinuities in construction lifts and external loads on the concrete behaviour. Nevertheless, the early-age behaviour of the so-called gusset, which refers to the first construction stage after the raft foundation which also had an increased wall thickness compared to the rest of the inner containment wall, was

of particular interest. The corresponding locations of the designated sensors were as follows: G1 and F1 were top and bottom of the "gusset", respectively, and close to inner concrete surface, whilst G2 and F2 were top and bottom of the "gusset", respectively, and at mid-thickness of the section.

Acknowledgements The kind contribution of Benoit Masson, Alexis Courtois and François Martinot from EDF France for sharing their experience on VeRCoRS is gratefully acknowledged. Regarding the monitoring programme "ground slab Boxberg", we wish to thank MPA Braunschweig for the very professional technical support in the installation of the monitoring programme on-site as well as Vattenfall for the financial assistance.

Other work was partially supported by: project POCI-01-0145-FEDER-007633 (ISISE), funded by FEDER funds through COMPETE2020-Programa Operacional Competitividade e Internacionalização (POCI) and by Portuguese funds through FCT—Fundação para a Ciência e a Tecnologia. FCT and FEDER (COMPETE2020) are also acknowledged for the funding of the research project IntegraCrete PTDC/ECM-EST/1056/2014 (POCI-01-0145-FEDER-016841).

References

ASCE. (2000). Guidelines for instrumentation and measurements for monitoring dam performance. Report by the ASCE Task Committee on instrumentation and monitoring dam performance, USA.

Acerbis, R., Asche, H., Barbieri, G., & Collotta, T. (2011). Recommendations for converting strain measured in concrete to stress. *Geotechnical Instrumentation News, 65,* 29–33.

ACI Committee 305. (2007). *Specifications for hot weather concreting*. U.S.A.: The American Concrete Institute.

ASTM. (1993). Manual on the use of thermocouples in temperature measurement. ASTM Committee E20 on temperature measurement (4th ed.), ASTM manual series MNL 12. U.S.A.: ASTM International.

ASTM. (2015). ASTM G167-15, Standard test method for calibration of a pyranometer using a pyrheliometer. U.S.A.: ASTM International.

Austin S. A., Robins P. J., & Bishop, W. J. (2006). Instrumentation and early-age monitoring of concrete slabs. *Proceedings of the Institution of Civil Engineers – Structures and Buildings*, *159*(SB4), 187–195.

Azenha, M. (2009). Numerical simulation of structural behaviour of concrete since its early ages. Ph.D. thesis, Faculdade de Engenharia da Universidade do Porto.

Azenha, M., Faria, R., & Ferreira, D. (2009). Identification of early-age concrete temperatures and strains: Monitoring and numerical simulation. *Cement & Concrete Composites, 31,* 369–378.

Azenha, M., Faria, R., & Figueiras, H. (2011). Thermography as a technique for monitoring early age temperatures of hardening concrete. *Constructions and Building Materials, 25*(11), 4232–4240.

Azenha, M., Lameiras, R., de Sousa, C., & Barros, J. (2014). Application of air cooled pipes for reduction of early age cracking risk in a massive RC wall. *Engineering Structures, 62–63,* 148–163.

Azenha, M., Leitao, L., Granja, J. L., de Sousa, C., Faria, R., & Barros, J. A. O. (2017). Experimental validation of a framework for hygro-mechanical simulation of self-induced stresses. *Cement and Concrete Composites, 80*, 41–54.

Bagavathiappan, S., Lahiri, B. B., Saravanan, T., Philip, J., & Jayakumar, T. (2013). Infrared thermography for condition monitoring—A review. *Infrared Physics & Technology, 60*, 35–55.

Bamforth, P. B. (2007). *CIRIA660: Early-age thermal crack control in concrete*. London: CIRIA.

Bao, X., & Chen, L. (2012). Recent progress in distributed fiber optic sensors. *Sensors, 2012*(12), 8601–8639. https://doi.org/10.3390/s120708601.

Barnes, R. (2016). *Interpretation of hygrometer readings for moisture in concrete floors*. Concrete Advice No. 29. Camberley, U.K.: The Concrete Society.

Barroca, N., Borges, L. M., Velez, F. J., Monteiro, F., Gorski, M., & Castro-Gomes, J. (2013). Wireless sensor networks for temperature and humidity monitoring within concrete structures. *Construction and Building Materials, 40*, 1156–1166.

Bazant, Z. P. (1972a). Numerical determination of long-range stress history from strain history in concrete. *Material and Structures, 5*, 135–141.

Bazant, Z. P. (1972b). Prediction of concrete creep effects using age-adjusted effective modulus method. *American Concrete Institute, 69,* 212–217.

Beck, Y. L., Kah, A. A., Cunat, P., Guidoux, C., Artieres, O., Mars, J., et al. (2010). Thermal monitoring of embankment dams by fiber optics. In *8th ICOLD European Club Symposium on Dam Safety*, Innsbruck, Austria.

Beck, Y. L., Martonot, F., Desforges, S., Buchoud, E., & Henault, J. M. (2016). Distributed measurements with optical sensors in the EDF group: experience feedback and perspectives. In R. J. Mair, K. Soga, Y. Jin, A. K. Parlikad & J. M. Schooling (Eds.), *Proceedings of the International Conference on Smart Infrastructure and Construction*, June, Cambridge, UK (pp. 3–8).

Bekowich, R. S. (1968). Instrumentation in prestressed concrete containment structures. *Nuclear Engineering and Design, 8*(4), 500–512.

Bernander, S. (1998). Practical measures to avoiding early age thermal cracking in concrete structures. In R. Springenschmid (Ed.), *Prevention of thermal cracking in concrete at early ages, RILEM Report 15* (pp. 255–314). London, U.K.: E & FN Spon.

Billon, A., Henault, J. M., Quiertant, M., Taillade, F., Khadour, A., Martin, R. P., et al. (2014). Quantitative strain measurement with distributed fibre optic systems: Qualification of a sensing cable bonded to the surface of a concrete structure. In *Proceedings of the EWSHM-7th European Workshop on Structural Health Monitoring*, Nantes, France, July 8–11.

Bofang, Z. (2014). *Thermal stresses and temperature control of mass concrete*. Oxford, UK: Elsevier/Butterworth-Heinemann.

Burton, T., Jenkins, N., Sharpe, D., & Bossanyi, E. (2011). *Wind energy handbook* (2nd ed.). West Sussex, U.K.: Wiley.

Carino, N. J., & Lew, H. S. (2001). The maturity method: From theory to application. In C. Chang (Ed.), *Proceedings of the Structures Congress and Exposition* (19 pp.), May 21–23, Washington D.C.: American Society of Civil Engineers.

Carlson, R. W. (1966). *Manual for the use of stress meters, strain meters, and joint meters in mass concrete* (3rd ed.). Berkeley, California, U.S.A.: Gillick & Co.

Chang, C. Y., & Hung, S. S. (2012). Implementation RFIC and sensor technology to measure temperature and humidity inside concrete structures. *Construction and Building Materials, 26,* 628–637.

Childs, P. R. N. (2001). *Practical temperature measurement*. Oxford, U.K.: Butterworth-Heinemann.

Choi, S., & Won, M. C. (2010). Thermal strain and drying shrinkage of concrete structures in the field. *ACI Materials Journal, 107*(5), 498–507.

Choi, S., Cha, S. W., & Oh, B. H. (2011). Thermo-hygro-mechanical behavior of early-age concrete deck in composite bridge under environmental loadings. Part 2: Strain and stress. *Materials and Structures, 44*(7), 1347–1367.

Choi, S. C., & Oh, B. H. (2010). New viscoelastic model for early-age concrete based on measured strains and stresses. *ACI Materials Journal, 107*(3), 239–247.

Chu, I., Lee, Y., Amin, M. N., Jang, B.-S., & Kim, J.-K. (2013). Application of a thermal stress device for the prediction of stresses due to hydration heat in mass concrete structure. *Construction and Building Materials, 45*, 192–198.

Conceição, J., Faria, R., Azenha, M., Mamede, F., & Souza, F. (2014). Early-age behaviour of the concrete surrounding a turbine spiral case: Monitoring and thermo-mechanical modelling. *Engineering Structures, 81,* 327–340.

Corbin, M., & Garcia, M. (2016). *International benchmark VeRCoRs 2015—Overview, synthesis and lessons learnt*. Villeurbanne, France: EDF SEPTEN.

Costa, Â. M. V. (2011). *Thermo-mechanical analysis of self-induced stresses in concrete associated to heat of hydration: A case study of the spillway of Paradela dam*. Guimarães: University of Minho. (in Portuguese).

Dally, W. J., & Riley, F. W. (2005). *Experimental stress analysis* (4th ed.). USA: College House Enterprises.

Davis. (2016). *Precision weather instruments*. California, U.S.A.: Davis Instruments, Hayward.

Delepine-Lesoille, S., Merliot, E., Boulay, C., Quetel, L., Delaveau, M., & Courteville, A. (2006). Quasi-distributed optical fibre extensometers for continuous embedding into concrete: design and realization. *Smart Materials and Structures, 15,* 931–938.

Delepine-Lesoille, S., Girard, S., Landolt, M., et al. (2017). France state of the art distributed optical fibre sensors qualified for the monitoring of the French underground repository for high level and intermediate level long lived radioactive wastes. *Sensors, 17*(6).

Delsys. (2017). Technical note 301: Synchronisation and triggering, Boston, U.S.A.

Delta Ohm. (2017). LP Silicon-Pyro 03. Environmental Analysis 18, Ceselle di Selvazzano, Italy (2 pp.).

Domski, J., & Katzer, J. (2015). An example of monitoring of early-age concrete temperatures in a massive concrete slab. In I. Major & M. Major (Eds.), *Selected practical and theoretical aspects of contemporary mechanics* (pp. 94–105). Czestochowa University of Technology.

Eierle, B., & Schikora, K. (2000). Zwang und Rissbildung infolge Hydratationswärme - Grundlagen, Berechnungsmodelle und Tragverhalten, Heft 512. Deutscher Ausschuss für Stahlbeton (in German).

Emilio, M. D. P. (2013). *Data acquisition systems—From fundamentals to applied design*. New York, U.S.A.: Springer.

EURAMET. (2011). Calibration of thermocouples, Version 2.1, EURAMET cg-8, Germany.

Faria, R., Azenha, M., & Figueiras, A. (2006). Modelling of concrete at early ages. Application to an externally restrained slab. *Cement & Concrete Composites, 28,* 572–585.

Geokon. (2015). Instruction manual—Model 4370 concrete stressmeter. Retrieved July 12, 2017, from http://www.geokon.com/content/datasheets/4370_Concrete_Stressmeter.pdf.

Geokon. (2017). Instruction Manual—Model 4200 series vibrating wire strain gages. Retrieved May 29, 2017, from http://www.geokon.com/content/manuals/4200-4202-4204-4210_Strain_Gages.pdf.

Geymayer, H. G. (1967). Strain meters and stress meters for embedment in models of mass concrete structures. Technical Report No. 6-811 US Army Corps of Engineers, Vicksburg, Mississippi, U.S.A.

Glisic, B. (2000). Fibre optic sensors and behaviour in concrete at early age. Ph.D. thesis, Ecole Polytechnique Federale de Lausanne, Switzerland.

Glisic, B., & Inaudi, D. (2007). *Fibre optic methods for structural health monitoring*. West Sussex, England, U.K.: Wiley.

Glisic, B., & Simon, N. (2000). Monitoring of concrete at very early age using stiff SOFO sensor. *Cement & Concrete Composites, 22,* 115–119.

Hagart-Alexander, C. (2010). Part III: Measurement of temperature and chemical composition—Temperature measurements. In W. Boyes (Ed.), *Instrumentation reference book* (4th ed.) (pp. 269–326). Oxford, U.K.: Elsevier/Butterworth-Heinemann.

Harris, G. H., & Sabnis, G. M. (1999). *Structural modelling and experimental techniques* (2nd ed.). USA: CRC Press.

Heimdal, E., Kanstad, T., & Kompen, R. (2001a). Maridal Culvert, Norway - field test I. Luleå Sweden: Luleå university of technology, department of civil and mining engineering. IPACS-report BE96-3843/2001:73-7. pp. 69. ISBN 91-89580-73-7.

Heimdal, E., Kanstad, T., & Kompen, R. (2001b). Maridal culvert, Norway - field test II. Luleå Sweden: Luleå university of technology, department of civil and mining engineering. IPACS-report BE96-3843/2001:74-5. pp. 20. ISBN 91-89580-74-5.

Heinrich, J. P., & Schlicke, D. (2016). Hardening-induced stresses in very thick concrete members—Insights from comprehensive FE-Studies. In *MSSCE2016* (*Service Life Segment*), Lyngby, Denmark.

Henault, J.-M. (2013). Methodological approach for performance and durability assessment of distributed fiber optic sensors: Application to a specific fiber optic cable embedded in concrete. Ph.D. thesis, Universite de Paris-Est, France.

Henault, J.-M., Salin, J., Moreau, G., Delepine-Lesoille, S., Bertand, J., Taillade, F., et al. (2011). Qualification of a truly distributed fiber optic technique for strain and temperature measurements in concrete structures. In *EPJ Web of Conferences, 12, AMP 2010—International Workshop on Ageing Management of Nuclear Power Plants and Waste Disposal Structures* (EFC Event 334 – Ontario, Canada) (8 pp.).

Hill, K. O., & Meltz, G. (1997). Fiber Bragg grating technology fundamentals and overview. *Journal of Lightwave Technology, 15*(8), 1263–1276.

Honorio, T. (2015). Modelling concrete behaviour at early-age: Multiscale analysis and simulation of a massive disposal structure. Ph.D. thesis, Ecole normale superieure de Cachan, France.

Humar, N., Zupan, D., & Kryzanowski, A. (2016). Fiber optic measurement of mass concrete at an early age—Case study. In M. M. Ali & P. Platko (Eds.), *Advances and Tends in Engineering Sciences and Technologies II, Proceedings of the 2nd International Conference on Engineering Sciences and Technologies*, July. High Tatras Mountains, Slovak Republic: CRC Press – Taylor & Francis Group (pp. 433–440).

Hunter, S. R. (2003). Wind speed measurement and use of cup anemometry, Recommended practices for wind turbine testing, International Energy Agency (IEA) programme for research and development on wind energy conversion systems, Paris, France.

Inaudi, D., & Glisic, B. (2006). Distributed fiber optic strain and temperature sensing for structural health monitoring. In P. J. S. Cruz, D. M. Frangopol & L. C. C. Neves (Eds.), *Proceedings of the 3rd International Conference on Advances in Bridge Maintenance, Safety Management and Life-Cycle Performance*, July, Porto, Portugal (8 pp.).

ISO. (1990). ISO 9060:1990: Solar energy—Specification and classification of instruments for measuring hemispherical solar and direct solar radiation.

Johnston, L. G. (2005). *Wind energy systems, electronic edition*. Manhattan, KS, U.S.A.

Jung, S. H., Choi, Y. C., & Coi, S. (2017). Use of ternary blended concrete to mitigate thermal cracking in massive concrete structures—A field feasibility and monitoring case study. *Construction and Building Materials, 137*, 208–215.

Kanare, H. M. (2005). *Concrete floors and moisture*. Illinois, U.S.A.: Portland Cement Association, Engineering Bulleting 119.

Kanavaris, F. (2017). Early age behaviour and cracking risk of concretes containing GGBS. Ph.D. thesis, Queen's University of Belfast, UK.

Kanavaris, F., Robinson, D., Soutsos, M., & Chen, J.-F. (2016). Prediction of the early age behaviour of the gusset of the nuclear containment vessel. In *1st International Workshop on the EDF Benchmark VeRCoRs*, March, Paris, France.

Kawaguchi, T., & Nakane, S. (1996). Investigations on determining thermal stress in massive concrete structures. *ACI Materials Journal, 93*(1), 96–101.

Kim, J., Luis, R., Smith, S. M., Figueroa, J. A., Malocha, D. C., & Nam, B. H. (2015). Concrete temperature monitoring using passive wireless surface acoustic wave sensor system. *Sensors and Actuators A: Physical, 224*, 131–139.

Kurata, Y., Shionaga, R., Takase, K., & Shimomura, T. (2009). Study on measurement of concrete stress in structural members by effective stress meter. In Tanabe et al. (Eds.), *Creep, shrinkage and durability mechanics of concrete and concrete structures* (Vol. 1, pp. 293–297). CRC Press.

Langreder, W. (2010). Wind resource and site assessment. In W. Tong (Ed.), *Wind power generation and wind turbine design* (pp. 49–88). Southampton, U.K.: WIT Press.

Lawrence, A. M., Tia, M., Ferraro, C. C., & Bergin, M. (2012). Effect of early age strength on cracking in mass concrete containing different supplementary cementitious materials:

Experimental and finite-element investigation. *Journal of Materials in Civil Engineering, 24*, 362–372.
Lawrence, A. M., Tia, M., & Bergin, M. (2014). Consideration for handling of mass concrete: Control of internal restraint. *ACI Materials Journal, 111*(1), 3–11.
Lee, B. (2003). Review of the present status of optic fiber sensors. *Optical fiber Technology, 9,* 57–79.
Lee, H.-S., Cho, M.-W., Yang, H.-M., Lee, S.-B., & Park, W.-J. (2014). Curing management of early-age concrete at construction site using integrated wireless sensors. *Journal of Advanced Concrete Technology, 12,* 91–100.
Mainstone, R. J. (1953). Vibrating Wire Strain Gauge for USe in longterm test on structures. *Engineering, 176,* 153–156.
Mata, J., Lajes Martins, L., Silva Ribeiro, A., Tavares de Castro, A., & Serra, C. (2015). Contributions of applied metrology for concrete dam monitoring. In *Hydropower'15*, Stavanger, Norway.
Mather, R. J. (2005). Beaufort wind scale. In E. J. Oliver (Ed.), *Encyclopedia of world climatology* (pp. 156–157). Dordrecht, The Netherlands: Springer.
Meanset. (2009). Anemometer calibration procedure, Version 2, Spain.
Met Office. (2010). Beaufort: National meteorological library and archive fact sheet 6—The Beaufort scale, Version 01, Exeter, Devon, U.K.
Meydbray, J., Emery, K., & Kurtz, S. (2012). Pyranometers, reference cells: the difference. *PC Magazine*, (04), 108–110.
Milovanovic, B., & Pecur, I. B. (2016). Review of active IR thermography for detection and characterization of defects in reinforced concrete. *Journal of Imaging, 2*(11), 27 pp.
MM (Micro-Measurements). (2014a). Strain gage selection: Criteria, procedures, recommendations, strain gages and instruments, Tech Note TN-505-4, August, Wendell, U.S.A.
MM (Micro-Measurements). (2014b). Surface preparation for strain gage bonding. Instruction Bulletin B-129-8, August, Wendell, U.S.A.
MM (Micro-Measurements). (2014c). Strain gage installations with M-Bond 200 Adhesive. Instruction Bulletin B-127-14, December, Wendell, U.S.A.
MM (Micro-Measurements). (2015). Strain gage installations for concrete structures, strain gages and instruments, Tech Tip TT-611, July, Wendell, U.S.A.
Morabito, P. (2001). Sluice gate—Brembo river—Italy—Field test. IPACS report BE96-3843/2001:76-1.
Morris, A. S., & Langari, R. (2016). *Measurement and instrumentation—Theory and application* (2nd ed.). Oxford, U.S.A.: Academic Press/Elsevier.
Myrvoll, F., Hansen, S. B., Roti, J. A., & Halvorsen, A. (2003). *Field measurements in geomechanics*. Lisse (UK): Taylor Francis.
Nagataki, S. (1970). Shrinkage and shrinkage restraints in concrete pavements. *ASCE Structural Journal, ST7*, 1333–1358.
Nakra, B. C., & Chaudhry, K. K. (2016). *Instrumentation, measurement and analysis* (4th ed.). New Delhi, India: McGraw-Hill.
Neville, A. (2011). *Properties of concrete* (5th ed.). Harlow, England, UK: Pearson Education Limited.
Nietner, L., Schlicke, D., & Tue, N. V. (2011). Berücksichtigung von Viskoelastizität bei der Beurteilung von Zwangbeanspruchungen erhärtender Massenbetonbauteile. *Beton- und Stahlbetonbau, 106*, 169–177. https://doi.org/10.1002/best.201000051 (in German).
Nilsson, L. O. (1996). Interaction between microclimate and concrete—A prerequisite for deterioration. *Construction and Building Materials, 10*(5 Spec. Issue), 301–308.
Norris, A., Saafi, M., & Romine, P. (2008). Temperature and moisture monitoring in concrete structures using embedded nanotechnology/microelectromechanical systems (MEMS) sensors. *Construction and Building Materials, 22,* 111–120.
Omega Engineering. (1999). Practical strain gage measurements. Application note 290-1, U.S.A.
Omega Engineering. (2000). Practical temperature measurements. Application note, Agilent Technolgies, U.S.A.

Oukhemanou, E. (2016). Monitoring system. In *1st International Workshop on the EDF Benchmark VeRCoRs*, March, Paris, France.

Oukhemanou, E., Desforges, S., Buchoud, E., Michel-Ponnelle, S., & Courtois, A. (2016). VeRCoRs Mock-Up: Comprehensive monitoring system for reduced scale containment model. In *3rd Conference on Techonological Innovation in Nuclear Civil Engineering (TINCE-2016)*, September, Paris, France.

Paulescu, M., Paulescu, E., Gravila, P., & Badescu, V. (2013). *Weather modelling and forecasting of PV systems operation*. London, U.K.: Springer.

Poblete, M., Salshilli, R., Valenzuela, R., Bull, A., & Spratz, P. (1988). Field evaluation of thermal deformations in undowelled PCC pavement slabs. *Transportation Research Record, N., 1207,* 217–228.

Raphael, J. M., & Carlson, R. W. (1965). *Measurement of structural actions in dams* (3rd ed.). Berkeley, California, U.S.A.: Gillick & Co.

Reinhardt, H.-W. (2014). Aspects of imposed deformation in concrete structures—A condensed overview. *Structural Concrete, 15,* 454–460. https://doi.org/10.1002/suco.201400014.

Richardson, J. T. (1959). The structural behavior of Hungry Horse Dam. Engineering Monographs No. 24, US Department of the Interior Bureau of Reclamation, Denver, Colorado.

Riding, K. A., Poole, J. L., Schindler, A. K., Juenger, M. C. G., & Folliard, K. J. (2006). Evaluation of temperature prediction methods for mass concrete members. *ACI Materials Journal, 103*(25), 357–365.

Riding, K. A., Poole, J. L., Schindler, A. K., Juenger, M. C. G., & Folliard, K. J. (2009). Effects of construction time and coarse aggregate on bridge deck cracking. *ACI Materials Journal, 106* (5), 448–454.

RILEM Report 15. (1998). Prevention of thermal cracking in concrete at early ages (R. Springenschmid Ed.). RILEM Report 15. E & FN Spon, London, UK. ISBN 0 419 22310 X.

Rocha, M. (1965). In situ strain and stress measurements. In *Stress analysis, recent developments in numerical and experimental analysis*, Chapter 17 (pp. 425–461). London: Wiley.

Rogers, A. (1999). Review article: Distributed optical-fibre sensing. *Measurement Science Technology, 10*(8), R75–R99.

Rostásy, F. S., & Henning, W. (1990). Zwang und Rissbildung in Wänden auf Fundamenten, Heft 407. Deutscher Ausschuss für Stahlbeton (in German).

Rostásy, F. S., Krauß, M., Laube, M., Rusack, T., & Budelmann, H. (2007). Online-Monitoring und Berechnung der Betonspannungen infolge thermischen Zwangs für ein Trogbauwerk am Hauptbahnhof Berlin. *Bautechnik, 84*, 235–242. https://doi.org/10.1002/bate.200710020 (in German).

RST Instruments. (2017). Carlson strain meter. Retrieved May 29, 2017, from http://www.rstinstruments.com/Carlson-Strain-Meter.html.

Schlicke, D. (2014). Mindestbewehrung für zwangbeanspruchten Beton. Dissertation, 2. Aufl., Graz University of Technology (in German).

Schlicke, D. (2015). Lessons learned from in-situ measurements in hardening concrete members. In *2nd Workshop of COST Action TU1404 with Focus on Modelling of Cement-based Materials and Structures* (pp. 372–386). Presentations e-Book. https://doi.org/10.5281/zenodo.46070.

Schlicke, D., & Tue, N. V. (2015). Minimum reinforcement for crack width control in restrained concrete members considering the deformation compatibility. *Structural Concrete, 16,* 221–232. https://doi.org/10.1002/suco.201400058.

Sellers, B. (2003). The measurement of stress in concrete. In F. Myrvoll (Ed.), *Proceedings of 6th International Symposium in Field Measurements in Geomechanics* (pp. 643–656). Oslo, Norway.

Shahawy, M. A., & Arockiasamy, M. (1996). Field instrumentation to study the time-dependent behavior in sunshine skyway bridge. *Journal of Bridge Engineering. ASCE, 1*(2), 76–86.

Shi, N., Chen, Y., & Li, Z. (2016). Crack risk evaluation of early age concrete based on the distributed optical fiber temperature sensing. In *Advances in materials science and engineering* (Vol. 2016, 13 pp.).

Simpson, D. (2016). *Moisture in concrete floors*. Concrete Advice No. 22. Camberley, U.K.: The Concrete Society.

Snell, L. M. (2015). Monitoring temperatures in concrete construction using IR thermometers. *Concrete International, 37*(1), 57–63.

Soutsos, M., Hatzitheodorou, A., Kwasny, J., & Kanavaris, F. (2016). Effect of in situ temperature on the early age strength development of concretes with supplementary cementitious materials. *Construction and Building Materials, 103,* 105–116.

Soutsos, M., Hatzitheodorou, A., Kanavaris, F., & Kwasny, J. (2017). Effect of temperature on the strength development of mortar mixes with GGBS and fly ash. *Magazine of Concrete Research, 69*(15), 787–801.

Tanabe, T. (1998). Measurement of thermal stresses in situ. In R. Springenschmid (Ed.), *RILEM Report 15—Prevention of thermal cracking in concrete at early ages* (pp. 251–254). London: E & FN Spon.

TGES (The German Energy Society). (2008). *Planning and installing photovoltaic systems—A guide for installers, architects and engineers* (2nd ed.). Berlin, Germany: Earthscan.

Tong, A. (2001). Improving the accuracy of temperature measurements. *Sensor Review, 21*(3), 193–198.

Torrent, R. J., & Fucaraccio, J. R. (1982). Appropriate experimental techniques for the control of thermal cracking in large concrete masses. In *International Conference on Temperature Effect on Concrete and Asphaltic Concrete*, Baghdad.

Tue, N. V., Schlicke, D., & Bödefeld, J. (2007). Beanspruchungen in dicken Bodenplatten infolge des Abfließens der Hydratationswärme. *Bautechnik, 84*, 702–710. https://doi.org/10.1002/bate.200710060 (in German).

Tue, N. V., Schlicke, D., & Schneider, H. (2009). Zwangbeanspruchung massiver Kraftwerks-Bodenplatten infolge der Hydratationswärme. *Bautechnik, 86*, 142–149. https://doi.org/10.1002/bate.200910013 (in German).

Ukil, A., Braendle, H., & Krippner, P. (2011). Distributed temperature sensing: Review of technology and applications. *IEEE Sensors Journal, 12*(5), 885–892.

van Breugel, K. (1998). Prediction of temperature development in hardening concrete. In R. Springenschmid (Ed.), *RILEM Report 15 – Prevention of thermal cracking in concrete at early ages* (pp. 51–75). London, UK.

Vollpracht, A., Soutsos, M., & Kanavaris, F. (2018). Strength development of GGBS and fly ash concretes and applicability of fib model code's maturity function—A critical review. *Construction and Building Materials, 162,* 830–846.

Weil, J. G. (2004). Infrared thermographic techniques. In V. M. Malhotra & N. J. Carino (Eds.), *Nondestructive testing of concrete* (2nd ed.) (pp. 15/1–15/14). CRC Press.

WMO. (2008). *Guide to meteorological instruments and methods for observation* (No. 8, 7th ed.).

Wojcik, G. S., Fitzjarrald, D. R., & Plawsky, L. J. (2003). Modelling the interaction between the atmosphere and curing concrete bridge decks with the SLABS model. *Meteorological Applications, 10*(2), 165–186.

Wojcik, G. S. (2001). The interaction between the atmosphere and curing concrete bridge decks. Ph.D. thesis, State University of New York at Albany, U.S.A.

Yeon, J. H., Choi, S., & Won, M. C. (2013). In situ measurement of coefficient of thermal expansion in hardening concrete and its effect on thermal stress development. *Construction and Building Materials, 38,* 306–315.

Zreiki, J., Bouchelaghem, F., & Chaouche, M. (2010). Early-age behaviour of concrete in massive structures, experimentation and modelling. *Nuclear Engineering and Design, 240,* 2643–2654.